A new systematic approach using the Modified Gaussian Model: Insight for the characterization of chemical composition of olivines, pyroxenes and olivine-pyroxene mixtures

Harold Clénet, Patrick Pinet, Yves Daydou, Frédérick Heuripeau, Christine Rosemberg, David Baratoux, Serge Chevrel

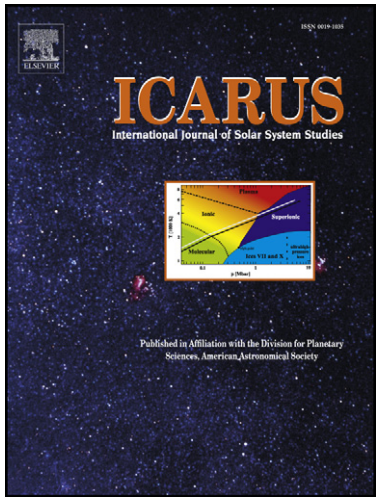

A new systematic approach using the Modified Gaussian Model: Insight for the characterization of chemical composition of olivines, pyroxenes and olivine-pyroxene mixtures

Harold Clénet, Patrick Pinet, Yves Daydou, Frédérick Heuripeau, Christine Rosemberg, David Baratoux, Serge Chevrel

PII: S0019-1035(11)00086-8
DOI: 10.1016/j.icarus.2011.03.002
Reference: YICAR 9745

To appear in: *Icarus*

Received Date: 8 October 2010
Revised Date: 11 January 2011
Accepted Date: 1 March 2011

Please cite this article as: Clénet, H., Pinet, P., Daydou, Y., Heuripeau, F., Rosemberg, C., Baratoux, D., Chevrel, S., A new systematic approach using the Modified Gaussian Model: Insight for the characterization of chemical composition of olivines, pyroxenes and olivine-pyroxene mixtures, *Icarus* (2011), doi: 10.1016/j.icarus.2011.03.002

A new systematic approach using the Modified Gaussian Model: Insight for the characterization of chemical composition of olivines, pyroxenes and olivine-pyroxene mixtures

Harold Clénet[1,2*], Patrick Pinet[1,2], Yves Daydou[1,2], Frédérick Heuripeau[1,2], Christine Rosemberg[1,2], David Baratoux[1,2], Serge Chevrel[1,2]

(1) Université de Toulouse, Observatoire Midi-Pyrénées, UPS-OMP, DTP/IRAP, Toulouse, France.
(2) CNRS; DTP/IRAP; 14, avenue Edouard Belin, F-31400 Toulouse, France

* Corresponding author: h.clenet@gmail.com, Phone: +33 4 72 44 62 35
Now at : Laboratoire de Sciences de la Terre, UCBL/ENS/CNRS
Bâtiment GEODE, 2 rue Raphael Dubois, 69622 Villeurbanne, France

Abstract

An automatic procedure has been implemented on the original MGM approach (Sunshine et al., 1990) in order to deal with an a priori unknown mafic mineralogy observed in the visible-near infrared by reflectance spectroscopy in the case of laboratory or natural rock spectra. We consider all the mixture possibilities involving orthopyroxene, clinopyroxene and olivine, and use accordingly for each configuration different numbers of Gaussians, depending on the potential complexity of the mixture. A key issue is to initialize the MGM procedure with a proper setting for the Gaussians parameters. An automatic analysis of the shape of the spectrum is first performed. The continuum is handled with a second order polynomial adjusted on the local maxima along the spectrum and Gaussians parameters initial settings are made on the basis of laboratory results available in the literature in the case of simple mixtures of mafic minerals. The returned MGM solutions are then assessed on spectroscopic grounds and either validated or discarded, on the basis of a mineralogical sorting.

The results presented in this paper are a first quantitative step to characterize both modal and chemical compositions of pyroxenes and olivines. A demonstration of the methodology on specific examples of binary and ternary olivine-pyroxenes mixtures has been made, which shows that the different non-linear effects which affect the Gaussian parameters (center and strength) can be successfully handled. Of note is the fact that the band center positions associated with the different mafic minerals are not set here in the inverse problem, and thus the MGM outputs are truly informative of the chemical composition of pyroxenes and olivines. With the consideration of some limits on the detection thresholds, these results are quite promising for increasing the operational use of the Modified Gaussian Model with large hyperspectral data sets in view of establishing detailed mineralogical mappings of magmatic units.

Keywords: Reflectance spectroscopy, Mineralogy, Spectral deconvolution, MGM

1. Background

In the field of reflectance spectroscopy, determination and characterization of mafic mineralogies have been a major area of investigation for the last 30 years (e.g., Adams, 1974; Mc Cord et al., 1981; Singer, 1981; Cloutis and Gaffey, 1991; Bishop et al., 1998; Harloff and Arnold, 2001; Schade et al., 2004; Pompilio et al., 2007). A progressive amount of complexity has been introduced in the description of spectra with the aim of extracting the relevant spectral information (e.g., albedo, slope of the continuum, position and depth of the absorption bands…) for mineralogy purposes.

Though its physical meaning is not thoroughly understood, the continuum plays an important role in all spectral analyses and particularly in MGM deconvolution (e.g., Clark and Roush, 1984; Harloff and Arnold, 2001; Clark et al., 2003). It is of particular relevance to define a continuum close to the spectrum global shape in order to best isolate the absorbing features at all wavelength.

1.1 Olivine and pyroxene spectroscopy

In visible and near-infrared reflectance spectra, olivine and pyroxenes are characterized by their Fe^{2+} electronic transition absorption bands. For a perfect octahedral crystal field, the electronic transition creates an absorption feature with a minimum around 1.10 µm. However, absorptions of a same metallic ion can occur at different wavelengths because of variations in the crystallographic site symmetry, bond type and length and site distortion (Burns, 1993) and absorption width is linked to thermal vibrations that modify the bond length around a mean value (Burns, 1993).

Consequently, pyroxenes reflectance spectra show two main absorptions respectively around 1 and 2 µm and a less pronounced absorption at 1.2 µm (Hunt and Salisbury, 1970; Adams, 1974, 1975; Singer, 1981; Klima et al., 2007). This 1.2 µm absorption is the result of molecular distortion in the M_1

crystallographic site (Burns, 1993). Nevertheless, clinopyroxene spectra are much more variable than orthopyroxene spectra and two main spectral types have been identified (Adams, 1975). Absorptions of spectral type B, much more common in most geological settings, correspond to those described above. Spectral type A clinopyroxene, where there are major contributions from ferrous iron in the M_1 site will results in absorption band near 0.9 and 1.15 µm and no band at 2 µm (Adams, 1975; Cloutis and Gaffey, 1991). Spectra of olivine are dominated by a broad complex absorption feature which is a composite of several absorptions: two of them correspond to iron in the M_1 site (around 0.85 and 1.25 µm) while the third one, around 1.05 µm, corresponds to the M_2 site (Burns, 1970; Hunt, 1977).

The substitution of different sized cations, such as calcium, iron and magnesium, also controls the positions of the different absorptions minima. In the case of olivine [$(Mg,Fe)_2SiO_4$], solid-solution ranges from forsterite to fayalite. The overall position of the 1.0 µm absorption feature is known to shift toward longer wavelengths with increasing iron content (Burns, 1970, 1993; Adams, 1975; King and Ridley, 1987). For pyroxenes [$(Ca,Mg,Fe)_2Si_2O_6$], wavelengths shift is function of Fe/(Mg+Fe+Ca) ratio (Adams, 1974, 1975; Cloutis et al., 1986; Cloutis et Gaffey, 1991). Basically, enstatite (orthopyroxene) main absorptions occur around 0.90 and 1.85 µm, while diopside (clinopyroxene) main absorptions occur around 1.00 and 2.30 µm (Hunt and Salisbury, 1970; Adams, 1974, 1975; Singer, 1981). The difference between the two types of pyroxenes is related to Fe^{2+} position: metallic ion is located preferentially in M_2 site for orthopyroxene and in M_1 site for clinopyroxene, Ca^{2+} being in M_2 site in the second case (Adams, 1974; Burns, 1993). In the case of orthopyroxene endmember (enstatite-ferrosilite), as there is almost no calcium in the structure, the wavelength shift is directly function of the Fe/(Mg+Fe) ratio. Hazen et al. (1978), followed by Cloutis and Gaffey (1991), have shown that absorption features evolve progressively between the pyroxenes endmember, absorption minima shifting to longer wavelength with increasing Fe content (diopside to hedenbergite and enstatite to ferrosilite) and Ca content (enstatite - pigeonite - augite - diopside).

On these grounds, the retrieval of characteristics of mafic minerals from unknown reflectance spectra does not appear as an impossible task and would be indeed of great use for the remote mineralogical analysis of planetary surfaces. However, today the direct interpretation of a spectrum is still limited as it is hampered by the overlap of the absorption features, particularly when there is a mixture of two or three minerals, as it is frequently the case with rocks. Indeed, such spectra show intermediate properties to the different endmember components. Those properties vary non-linearly as a function of minerals relative abundance and composition (Adams, 1974; Singer, 1981; Cloutis and Gaffey, 1991) and the key issue is to be able to deconvolve unambiguously a complex spectral shape measured either on a laboratory sample or from orbit, in order to detect and characterize the different endmember components. The Modified Gaussian Model (MGM), developed by Sunshine et al. (1990), has the potential to resolve the endmember contributions.

1.2 Use of the Modified Gaussian Model (MGM) for mafic mineral assemblages

The principle of the Modified Gaussian Model is to deconvolve overlapping absorptions of mafic mineral spectra into their fundamental absorption components. The specific interest of this model is to directly account for electronic transition processes (e.g., Sunshine et al., 1990). Consequently, the MGM approach is in essence able to achieve a direct detection and quantification of minerals which make up the observed surface.

The pioneering work by Sunshine et al. (1990) relies on the fact that spectrum variations in visible and near-infrared are caused by absorption features that can be described by means of Gaussians (Clark and Roush, 1984). Sunshine et al. (1990) used modified Gaussians to obtain a mathematical solution closer to the physical reality. Each Gaussian is parameterized by a band center, band width and band strength. As described in Sunshine and Pieters (1993), MGM computations are carried out in energy and natural log reflectance space. Thereby, overlapping absorptions are additive and can be modeled using linear inverse theory. The method applied is the stochastic inversion of Tarantola and Valette (1982) that permits the introduction of a priori information as constraints on the solutions. These constraints are defined by means of uncertainties, applied on each starting parameter and set as a function of considered absorptions. During the non-linear least-squares iterative process, Gaussians and continuum parameters vary until the residual errors are minimized (Sunshine et al., 1990; Sunshine and Pieters, 1993). The residual errors are calculated as the difference between the log of the actual spectrum and the log of the modeled spectrum. Spectra are modeled in the logarithm of reflectance space as a sum of modified Gaussian distributions superimposed on a baseline continuum. The resulting combinations of Gaussians can then be interpreted in terms of mineralogy.

Sunshine and Pieters (1993, 1998) first results dealt with cases involving simple mafic mineralogies, i.e. either olivine alone or pyroxenes only mixtures. This work will be used as a reference in our following study. Using three Gaussians in their model, Sunshine and Pieters (1998) have been able to characterize systematic trends linked to M_1 and M_2 sites for olivine, with a progressive increase with higher iron content of both band center positions toward longer wavelength and of the 1.05 µm band intensity relative to the 1.2 µm feature. Widths did not show any special trend.

Sunshine and Pieters (1993) also studied mixtures of two pyroxenes with fixed chemical compositions and succeeded in deconvolving the suite of spectra in terms of endmember absorptions. They showed that while the center and width of the absorption bands did not depend on the mineral proportions, the relative abundances of the two pyroxene minerals could be directly linked to the Gaussians strength.

At first order, in the case of simple mineralogies, MGM is thus able to retrieve modal and/or chemical composition from an unknown spectrum. Successive studies have shown the interest of the MGM approach for planetary surface characterization (e.g., Mustard and Sunshine, 1995; Mustard et al., 1997; Noble et al., 2006; Kanner et al., 2007). However, one should note that for the reference studies, all the spectra used were acquired on controlled laboratory powder samples, with grain size between 24 and 250 µm. Kanner et al. (2007) have also pointed out that the MGM returned solutions were sensitive to some extent to the band centers initialization.

So far, more complex situations addressing complex mineralogies (i.e. olivine and pyroxene(s) and/or different pyroxene composition) and/or rock samples (e.g., Pompilio et al., 2007) have been little explored by the MGM approach at the exception of a few recent works (e.g., Pompilio et al., 2006; Pompilio et al., 2009; Parente and Bishop, 2006; Pinet et al., 2006, 2007, 2009; Clenet et al., 2008, 2009) and significant efforts have to be made in this direction for improving our capability of spectroscopic modeling and interpretation when dealing with real world observations of unknown mafic rock lithologies observed under natural conditions. Our goal here is to improve the capability of the MGM to realistically model complicated mafic mineralogies.

1.3 Laboratory data sets

Our present study relies on laboratory data of synthetic mixtures with different grain sizes and natural rocks, mainly taken in the Reflectance Experiment Laboratory (RELAB) database at Brown University. Measurements have been produced using a bidirectional near-infrared spectrometer (i=30° and e=0°) from 0.5 to 2.5µm (Pieters, 1983; Pieters and Hiroi, 2004).

Spectra include olivine ranging from forsterite to fayalite (including some of the data used by Sunshine et al. (1998)), different types of pyroxene alone and mixtures (including the ones from Sunshine et al. (1993) and part of Klima et al. (2007)). We also use olivine and orthopyroxene mixtures (Mustard and Pieters, 1989; Hiroi and Pieters, 1994).

2. Methodology

2.1 Initialization driven by mineral chemical composition with application to mineralogical mixtures

The Modified Gaussian Model code we use in this paper is the one described by Sunshine et al. (1990, 1999). It can be downloaded at http://www.planetary.brown.edu/mgm/. However, modifications about the continuum and the Gaussians characteristics, as well as an automation of the procedure, have been introduced. Specificities of our approach are described hereafter.

MGM directly takes into account electronic transition processes; consequently, the number of Gaussians which should be used for a given deconvolution directly depends on the number of absorption bands present in a spectrum. As described above, three Gaussians are needed to characterize either an olivine or a pyroxene. Each absorption feature has a center which may vary in a specific range as a function of the mineral chemical composition (Adams, 1974; Hazen et al., 1978; Cloutis and Gaffey, 1991; Sunshine and Pieters, 1998). In this paper, Gaussians will be named accordingly to their respective band center initialization (e.g. the Gaussian which models clinopyroxene absorption between 980 and 1050 nm will be named Gaussian “1000”). So, olivine absorptions will be modeled by Gaussians “850” (ranging between 840-900 nm), “1050” (1040-1075 nm) and “1250” (1200-1300 nm); spectral type B clinopyroxene absorptions by Gaussians “1000” (980-1050 nm), “1200” and “2150” (2050-2350 nm);

orthopyroxene absorptions by Gaussians "900" (895-970 nm), "1200" and "1800" (1800-2100 nm). In our approach, we do not consider spectral type A clinopyroxenes and "clinopyroxene" will further refer to spectral type B clinopyroxene.

Two additional Gaussians are also required to obtain physically realistic modeling. The first one, centered around 450 nm, is used to model the strong large absorption at shorter wavelength (i.e. charge transfer in ultraviolet). The second one, centered around 650 nm, may account for a small pyroxene absorption, especially in the case of composition close to diopside (Sunshine and Pieters, 1993; Klima et al., 2007). This absorption may be attributable to ferrous-ferric iron charge transfer (Cloutis, 2002). Both Gaussians also contribute stabilizing the overall shape of the continuum in the visible domain.

In the case of an unknown mafic rock, the strategy is to consider that all the combinations between the three different minerals are possible. A set of Gaussians, dedicated to a specific mineralogy, will be called further "configuration" (e.g. olivine configuration, orthopyroxene configuration, orthopyroxene-clinopyroxene configuration…). In our problem, the number of configurations amounts to seven. In the case of the simplest configurations, four or five Gaussians are required to model a spectrum (cf. Tab. 1). Additional Gaussians are added in the case of mixtures. However, identical Gaussians which appear for two or more minerals are used only once (i.e. absorption around 1200 nm for the two pyroxenes (Noble et al., 2006). Moreover, in the case of olivine-pyroxene mixtures, the pyroxene absorption around 1200 nm is masked by the olivine one. In this case, the choice is made for the time being not to use the Gaussian 1200 dedicated to pyroxene. Accordingly, nine Gaussians are used in the most complicated case which addresses a ternary mixture. The different combinations used for every configuration are reported in Table 1.

Following from what has been explained earlier in section 1.2, each Gaussian has to be initialized with a band center and an uncertainty on this parameter. The uncertainties on the Gaussians parameters have been set in such a way that our MGM modeling may encompass the range of spectral changes associated with chemical compositions of pyroxene and olivine. A number of tests have driven us to fix a band center uncertainty of 200 nm for all the Gaussians in the 1µm domain, and 400 nm in the 2 µm domain.

2.2 Initialization considering laboratory samples and natural rocks

2.2.1 Continuum

For laboratory data, the global shape of a spectrum is usually quite flat. The continuum, as defined by Clark and Roush (1984), was initially taken as a straight line. In the original version of the MGM, Sunshine and Pieters (1993) have chosen a continuum which is linear in energy. This continuum is controlled by two parameters, respectively linked to the slope and to the shift in reflectance. In wavelength space, such a continuum comes as a flat line in infrared and a curved line at shorter wavelengths.

In the present study, the undertaken MGM approach is intended to model laboratory spectra as well as natural rock spectra. As illustrated in Figure 1 for the case of diopside, the spectra of different grain-sized powders exhibit obvious differences from bulk rocks of a similar composition measured in the field. The physical rock texture is the major cause for these spectral differences. Laboratory spectra with larger grain size (>45µm) look more similar to the natural data than the small grain size spectrum (<45µm). The presence of varnish at the surface (e.g. desert varnish) may also contribute to the spectral signature in the case of natural rocks. The observed differences can be generally ascribed to photometric and environmental (e.g. varnish, alteration) or saturation effects (Combe et al., 2006; Pompilio et al., 2007; 2009; Roy et al., 2009). The general characteristics are as follows: i) variations of the reflectance mean level; ii) lower reflectance level at longest wavelength (i.e. around 2.5 µm); and iii) weaker relative strength of the spectral absorptions.

By definition, the variations of the reflectance mean level are handled by the continuum in the MGM deconvolution. For the second effect, tests have shown that a straight line continuum will significantly overestimate the infrared absorption(s) strength(s) in the case of natural rocks as the continuum is strongly controlled by the local maxima at 0.6-0.8 µm and 1.5-1.6 µm. The choice of a second order polynomial continuum in wavelength space clearly improves the situation. Such a continuum is defined by three parameters which correspond respectively to the average reflectance level, the global slope and the function curvature. That way, the overall shape of the continuum better describes the general spectral trend of any spectrum all along the visible-near infrared domain and as a result, Gaussians strength will better characterize the real absorption strength.

Though its physical meaning is not thoroughly understood, the continuum plays an important role in all spectral analyses and particularly in MGM deconvolution (e.g., Clark and Roush, 1984; Harloff and Arnold, 2001; Clark et al., 2003). It is of particular relevance to define a starting continuum close to the spectrum global shape in order to best isolate the absorbing features at all wavelength. This is achieved from a spectral shape analysis, based on an automatic procedure detecting the local minima and maxima along the spectral domain (cf. Fig. 2). This information will also be quite useful for the initialization of the Gaussians to be used as described in section 2.2.3. The coefficients of the polynomial are set so that the starting continuum is defined as a smooth mathematical function. This function is constrained by the main maxima detected along the spectrum and used as anchor points, though the final continuum (after running the MGM) may not be necessarily tangential to the spectrum, with the advantage that its overall shape is not controlled by a restricted spectral range.

2.2.2 Influence of initialization on the MGM results

Consequently to the use of a generalized inversion approach, the MGM results are sensitive to Gaussians centers initializations, and a variation has been found between the MGM calculated absorption center and the real mineralogical absorption center (Kanner et al., 2007). In the case of laboratory data, variation ranges are on the order of ±8 and ±17 nm, respectively for the 1 µm and 2 µm domain

absorptions. As a complement, we assess in the following the influence of Gaussians strength initialization on the MGM results. The sensitivity of the MGM is here tested considering the initial strength of the Gaussians compared to the strength of the mineralogical absorptions. To do that, we make systematic tests considering those parameters. Principle and results are described hereafter.

For a given spectrum, we vary the initialization of the Gaussians strength parameter, all the Gaussians of the set having an identical initial strength. At the same time, we consider a series of synthetic spectra showing absorptions strengths ranging from "laboratory" case to "natural" case. To simulate the case of "natural" spectra (cf. Fig.1, i.e. keeping a strictly identical chemical composition but showing weaker absorptions), we choose to use laboratory spectra which are artificially flattened. Reflectance logarithm is thus multiplied by the same factor at all wavelengths. That way, the higher the flattening rate, the flatter the spectrum with a higher reflectance level. Examples of four synthetic spectra are shown in Figure 3-A. The laboratory reference spectrum considered here is a mixture of orthopyroxene and clinopyroxene, with particle size between 45 and 75 µm, taken from the Sunshine and Pieters (1993) set.

For all our tests (see graphs on Figures 3-B and 3-C), calculations are made by varying the flattening rate with a 1% step. Initial Gaussians strengths range from -0.3 to 0 by step of 0.05. Final centers and strengths are calculated using the MGM in all the parametric space and visualization is based on a color scale. High band center positions, or large strengths, correspond to red shade; conversely low band center positions, or weak strengths, correspond to blue shade. If initialization has no influence, results should show throughout the parametric space:

-i) the same value regarding the center of each Gaussian associated with a given absorption feature, close to the one determined by Sunshine and Pieters (1993) (with a possible variability on the order of that defined by Kanner et al. (2007));

-ii) a progressive decrease of the calculated strength as a function of the flattening rate, independent of the initialization strength.

We ran different simulations using varied pyroxenes mixture spectra and olivine alone spectra. In this paper, we only display the example resulting of the simulation based on the orthopyroxene/clinopyroxene mixture spectrum mentioned above. Figure 3-B represents the final center positions (i.e., after running the MGM) of the two orthopyroxene Gaussians in the 1 (left) and 2 (right) µm domains. For both diagrams, one can clearly note variations across the parametric space. In the 1 µm domain, the center position presents a 180 nm difference between the maximum and the minimum values. The lowest center is found when a flat spectrum is modeled with high initial strength; conversely the highest center is found when a spectrum showing well defined absorptions is modeled with low initial strength. The overall regular spacing between two contiguous contour lines indicates a progressive shift. In the 2 µm domain, the center final position varies between 1600 and 1850 nm, following a similar trend to the 1 µm domain. One should note however that beyond a particular ratio between the initial Gaussian strength and the strength of the absorption, values of the center final position are more stable (upper left part of the diagram). Though not shown here, results in the case of clinopyroxene Gaussians show

basically a similar behavior, with a reversed trend, i.e. the highest center positions are associated with a flat spectrum combined with high initial strength.

The calculated Gaussians strength evolution has also been documented (see graphs on figure 3-C). Contour lines can be separated in two areas, the limit being the first diagonal of the graph. In the upper left triangle, contour lines are closer to horizontal and regularly spaced out. It means that, independently of the initialization, final Gaussians strengths are only function of the flattening rate, i.e. the strength of the mineralogical absorption. On the other hand, in the lower right triangle part of the graph, contour lines are curved downward and tend to be vertical, which implies that this time the final Gaussians strengths are only function of the initialization strength. Similar trends are once again observed in the case of clinopyroxene Gaussians. Those results highlight that for both centers and strengths, a special attention must be put on the initialization of Gaussians parameters. Similar conclusions are drawn when different orthopyroxene/clinopyroxene ratios and various grain sizes are considered on the basis of the Sunshine and Pieters (1993) set of spectra.

A series of olivine spectra from the Sunshine and Pieters (1998) set has also been examined. It is found that the results are less dependent on the initialization setting. Final centers appear to be shifted only when the flattening rate and the initial strength are high. In such case, as for pyroxenes, results cannot be related to mineralogical information.

The last aspect of our assessment deals with the uncertainties on the initial strength parameters and shows that a variation of these uncertainties has no major influence on the MGM deconvolution process. In the following, these uncertainties will be taken such as they will be an order of magnitude larger for band centers, on the same order for band widths, and an order of magnitude less for band strengths than in earlier studies (Sunshine and Pieters, 1993; Sunshine et al., 1998). These results suggest that one may relax the constraints set on the band center without doing any harm to the solution.

In conclusion, this section shows that the MGM initialization phase cannot be carried out in a blind way and that the MGM modeling cannot be used automatically on a complex data set (e.g. airborne or orbital data) without some careful settings. As an example, data from Sunshine and Pieters (1993) indicate that the orthopyroxene endmember absorptions are located around 907 and 1827 nm (represented by dashed lines on Fig.3). These results can only be obtained with specific combinations of the initial Gaussians strength versus the flattening rate (e.g. for a 50% flattening rate, strength initialization should be close to -0.30 while for a 80% rate, it should be close to -0.12). For too weak absorptions (simulated by a flattening rate of 80% or more), it may happen that the MGM deconvolution returns results unrelated to the mineralogical information. This case apart, a first-order linear relation is found between the two parameters. This fact will be used in the next section to automatically initialize the MGM.

2.2.3 Automatic initialization of the Gaussians parameters

Considering a spectrum of an unknown mafic assemblage, one cannot choose a priori a given mineralogical configuration among the seven possible ones. The first step of our automatic initialization

consists in the analysis of the spectrum global shape (cf. section 2.2.1). The spectrum maxima and minima are used to estimate the measured absorption strengths and widths (Figure 2), with the strength estimate defined as the difference between the reflectance minimum and a straight line linking the adjacent maxima and the measured width estimate defined as the width at half strength. As a result, the general characteristics of a spectrum can be described by four parameters. The next step of the initialization is then to link for a given mineralogical combination those parameters to expected values for the Gaussians as defined in the literature.

As we consider the seven possible mineralogical associations, the meaning of the four measured parameters may differ. In the case of a single pyroxene, interpretation is easy as each Gaussian is directly related to the combination of the measured strength and width. In the case of olivine, the three Gaussians overlap and the case appears more complex. However, results from Sunshine and Pieters (1998) established relationships between the three Gaussians. On this basis of knowledge, a partitioning is made between the Gaussians, the strength and width of Gaussians “850” and “1050” being calculated as a function of the “1250” one for which parameters initialization depends on the 1 µm measured absorption feature and on the Sunshine and Pieters (1998) results.

In the case of a pyroxene mixture, several steps must be used. Indeed, whatever the pyroxene composition, Gaussians in the 1 µm and 2 µm domains overlap without obvious relationships. First, a first order linear approximation is drawn between the position of the reflectance minimum in the 1 µm domain and the mixture composition. This is established on the basis of the Sunshine et al. (1993) dealing with seven compositions and three grain sizes. In a second step, we calculate from the results of the literature the relative strength of the orthopyroxene Gaussian compared to the clinopyroxene one in the 1 µm domain. Figure 4-A shows that the relation is non-linear, orthopyroxene strength being generally more important than the clinopyroxene strength. In addition, one notes that when orthopyroxene represents more than 65% of the mixture, the grain size has a drastic effect on the OPX/CPX strength ratio. To take into account those constraints, the choice has been made to split the mixture composition range in five intervals (below 10% of orthopyroxene, only clinopyroxene absorptions can be resolved, while above 90% of orthopyroxene, only orthopyroxene absorptions can be resolved). For each of them, a characteristic ratio is fixed and will be used further (e.g. Cpx strength/Opx strength ratio varies from 2/1 to 1/12, see Figure 4-A for details). At this time, the relative strength parameters are settled in the 1 µm domain. We now have to link the orthopyroxene Gaussian strength defined by Sunshine and Pieters (1993) and the absorption feature strength measured on the spectrum. Such a relation can be approximated to first-order by a linear regression, with some fluctuations caused by grain size effects. This relationship permits us to initialize efficiently the different Gaussians. Finally, a ratio, based on Sunshine and Pieters (1993) results, is defined which permits us to initialize the 2 µm Gaussians band strength as a function of the 1 µm Gaussians band strength (Figure 4-B). These empirical ratios (opx_1/opx_2, cpx_1/cpx_2) are determined within five distinct intervals of mixture composition for both ortho- and clinopyroxene, respectively (see Figure 4-B). As a result, all the Gaussian strengths in the 1 and 2 µm

domains can be initialized from one measured parameter on the spectrum that is the depth of the 1 µm feature. A similar approach is developed for the width parameters.

For olivine-pyroxene mixtures, no systematic study of the MGM behavior as a function of the relative proportions of the mineral constituents is available so far to initialize the Gaussians parameters. For the olivine-orthopyroxene mixture, we used a set of 5 spectra found in the RELAB library (from Mustard and Pieters (1989) and Hiroi and Pieters (1994) (see also in section 3.2.1)). Thus, Gaussians parameters calculated by the MGM for a mineral alone are used as a reference in the mixture case. Then, the steps described for the pyroxene mixtures are repeated with the introduction of the three coupled Gaussians in the 1 µm domain for the olivine as detailed above. Next, we extrapolate those new results to olivine-clinopyroxene mixtures. We here used a set of spectra acquired on the field in Oman's ophiolite with an ASD FieldSpec® 3 field spectrometer. They do not span however the full range of olivine/clinopyroxene possible mixtures and are mostly used as a first-order estimate to calibrate the Gaussians parameters. Finally for the most complicated case (ternary mixtures of olivine-orthopyroxene-clinopyroxene), our experimental knowledge is limited as it relies on only three spectra of identical composition, with various grain sizes (spectra from Mustard et al. (1993) and Pieters et al. (1993)). Following Ockham's razor principle, all the Gaussian functions associated with the three minerals are initialized with an identical strength defined as one third of the measured depth of the 1 µm absorption feature of the spectrum.

The stability of the automatic initialization is assessed as previously demonstrated (see Fig. 3). MGM calculated parameters are directly plotted as a function of the flattening rate. Shown on Figure 5 are the results for a 50/50 pyroxene mixture (left) and 75/25 olivine-orthopyroxene mixture (right). We can see that for a flattening rate less than 80% those results are quite stable for center parameters, meaning that the case of very shallow absorption features excepted (which may require to set some threshold when dealing with an hyperspectral image), the MGM deconvolution is able to extract the mineralogical information. Figure 5 also shows that final Gaussians strengths vary linearly as a function of the flattening rate. However, as found in the case of Gaussian centers, when the absorption is too weak, parameters estimates should be taken cautiously. These situations set aside, our automatic initialization is able to process a wide range of natural spectra, with promising applications on large datasets.

2.2.4 Mineralogical sorting

As explained earlier, we run successively on an unknown spectrum the MGM with the seven configurations in order to test every possible combination of the three mafic minerals. Root-mean-square (*rms*) between model and observation is used as a mandatory convergence criterion. However, the potentially large number of Gaussian functions may result in low *rms* mathematical solutions without physical meaning. The next simple criterion consists in the rejection of solutions with positive band strengths (i.e., associated with spectral features "above" the continuum) indicative of a wrong modeling (due to the use of too many Gaussians for instance versus the number of real absorptions). The retrieved

mathematical solutions have then to be assessed on spectroscopic grounds and accordingly either validated or discarded. This final step is accomplished through a mineralogical sorting of the returned MGM results, keeping in mind that the modeled Gaussian functions must verify spectroscopic criteria to be validated in view of a mineralogical interpretation. As an example, for olivine, our MGM results show that the position of the three centers increases to longer wavelength with higher Fe content, as established in Sunshine et al. (1998). So, each Gaussian function must have its center between the minimum and the maximum values (e.g. between 0.81 µm and 0.94 µm for the "850" Gaussian). Similarly, the band widths have to satisfy to the experimental constraints set by Sunshine and Pieters (1998), with some margin based on the MGM uncertainties as defined by Kanner et al. (2007) and on the diversity of the laboratory spectra we have studied ourselves, including olivine with larger grain size and olivine/pyroxenes mixtures. Constraints on the relative strength of the different Gaussian functions are also used knowing that the "1250" absorption is always stronger than the "850" and "1050" ones (Sunshine and Pieters, 1998). Only if all those criteria are satisfied, can the MGM solution be validated as an indication of the presence of olivine.

We used the same approach in the case of pyroxene absorptions, relying on Adams (1974) and Sunshine and Pieters (1993) experimental data. For pyroxenes, in addition to the previous constraints, we add an additional rejection criterion based on the fact that the 1 and 2 µm absorption positions are coupled as shown by Adams (1974). However, it is to be reminded that pyroxene is a solid solution, with the implication that intermediate pyroxenes may present absorption features that can be interpreted both in terms of orthopyroxene and clinopyroxene. Moreover, minor amounts of elements such as Ti can modify the relative absorptions centers in the two wavelength domains, shifting the pyroxene position above Adams (1974) trends (Cloutis and Gaffey, 1991).

At the end of the mineralogical sorting process, three situations can occur:

-i) First, all the solutions are rejected. This means that either there are no mafic minerals in the analyzed rock or there is an additional spectrally active mineral which is not taken into account by our systematic procedure.

-ii) only one configuration matches all the constraints: this mathematical solution is physically realistic and Gaussian function parameters can be used to extract minerals characteristics.

-iii) two (or rarely more) configurations can be accepted. This effect depends on the characteristics of the minerals relative absorptions. For instance, pyroxene absorptions may hide olivine ones and in the case of a 50/50 olivine-orthopyroxene mixture, it appears that two configurations are validated (see Figure 6), all the other configurations being rejected as they fail at modeling properly the spectrum or they do not satisfy spectroscopic criteria associated with olivine and /or orthopyroxene mineral(s). When at least two configurations are kept, we will consider the most complicated mixture as the most representative to identify the presence of minerals.

In the first part of the paper, the implemented procedure has been described. In the following, it will be applied on different laboratory spectra to test its ability for:

-i) the detection of the presence of mafic minerals in a given assemblage;

-ii) the characterization of their chemical compositions.

3. Results

3.1 Case of simple mafic mineralogies

3.1.1 Olivine

Our approach is first validated in the case of olivine alone, using a set of 28 spectra from the RELAB library (cf. Table 2). Ten of them were used by Sunshine and Pieters (1998). The present set deals with a larger spectral variety than in Sunshine and Pieters (1998), both in terms of mean reflectance level and relative strength of the absorptions. Our systematic approach, including the seven configurations, has been applied to all spectra and in each case, only the olivine configuration is retained. MGM results are given (Fig. 7) for three compositions ($Fo_{96.9}$, $Fo_{50.5}$, $Fo_{0.1}$) spanning the whole range of the solid solution.

Gaussian function parameters are in general agreement with the trends defined by Sunshine and Pieters (1998), with widths and normalized strengths corresponding to those defined in the literature. As expected, both an increase of the Gaussian centers positions toward longer wavelengths correlated to the iron content and of the "1050" normalized intensity are observed. However, due to the choice of a second order polynomial continuum, weaker strengths in the case of the Gaussian "850" (i.e. between -0.4 and -0.6) are obtained. Indeed, the continuum presents a tight curvature at shorter wavelengths and thus better matches the overall shape of the spectrum than in the case of a straight line, with an effect on the relative "850" and "1050" strengths. Evolution of the three Gaussian centers position as a function of iron content is similar to Sunshine and Pieters (1998) results. However, the definition of a second-order polynomial continuum slightly modifies the relations established for the Gaussians center position. Accordingly, the three regression lines established by Sunshine and Pieters (1998) have been recalculated in order to derive the composition of an unknown olivine. The band center position for the "1250" Gaussian appears to be shifted by a few nanometers toward longer wavelengths with basically the same slope coefficient as in Sunshine and Pieters (1998).

Our work on laboratory data shows that olivine can be properly detected and compositionally characterized. However, when dealing with natural conditions, grains size may also affect the chemical characterization (e.g. Crown and Pieters, 1987; Mustard and Hays, 1997; Lucey, 1998). Results on Figure 8 (left) show indeed that large grains size forsterite have absorption characteristics that may mimic fayalite absorption features. This effect, not really documented in the literature, appears when the grains size exceeds 250 µm and for grains larger than 1 mm, approaching the case of rock slab, saturation may be reached (e.g., Pompilio et al., 2009). In this situation, MGM results can be ambiguous and large grain size forsterite might be interpreted as fayalite (Fig. 8 right). Consequently, interpretation of MGM results when considering an unknown olivine must be carefully taken. Indeed, in the absence of grain size

493 knowledge, olivine could have a lower Fe content than predicted by remote sensing, with significant
494 implications (e.g., Poulet et al., 2009a).
495
496 3.1.2 Pyroxenes
497
498 The case of monomineral pyroxenes is then examined for the purpose of validation. We used a set
499 of 19 spectra from the RELAB library. Twelve of them, the synthetic orthopyroxene suite (enstatite-
500 ferrosilite), were used by Klima et al. (2007). Other spectra present various compositions of natural
501 pyroxenes ranging from enstatite to diopside and hedenbergite (RELAB spectra references are mentioned
502 throughout the paper). Our systematic approach with seven configurations (cf. Table 1) has been applied
503 on the entire set. In most cases, only one mathematical solution issued for either orthopyroxene or
504 clinopyroxene configuration is retained. Figure 9 shows the MGM results for four compositions. One
505 should note that in the case of an intermediate pyroxene, e.g. with a pigeonite, both opx and cpx
506 configurations give similar mathematical solutions, consistent with the fact that the position of the band
507 centers associated with orthopyroxene and clinopyroxene may overlap each other (Adams, 1974).
508 For almost all the pyroxenes investigated here, the present MGM outputs are in agreement with
509 earlier results in the literature. However, for three spectra of our set, none of the seven mathematical
510 solutions corresponds to the expected trends. Those spectra are associated to hedenbergite, a Fe- and Ca-
511 rich pyroxene (in our case compositions are respectively $Wo_{49}En_4Fs_{47}$ (RELAB C1PP12), $Wo_{55}En_9Fs_{36}$
512 (RELAB C1PP14) and $Wo_{53}En_2Fs_{45}$ (RELAB C1SB15)), and correspond to spectral type A
513 clinopyroxenes (Wo close to or greater than 50 mol %; Cloutis and Gaffey, 1991). Indeed, as mentioned
514 previously, such minerals show a very strong absorption in the 1 µm domain with no absorption (or a
515 very subdued one) in the 2 µm domain. Schade et al. (2004) have shown that three dedicated Gaussian
516 functions, different from olivine ones, are then needed to model the 1 µm feature and no configuration
517 has been developed and tested so far in our approach to handle this case.
518 With this limitation in mind, we assess the performance and consistency of the MGM outputs
519 versus Adams (1974)'s results. First, one explores the spectral evolution associated with an iron content
520 variation in the case of a synthetic orthopyroxene series (Klima et al., 2007). For enstatite, absorptions are
521 centered around 900 and 1800 nm while they are centered around 920 and 1960 nm for $En_{50}Fs_{50}$ and 940
522 and 2070 nm for ferrosilite. A progressive shift (Fig. 10-A) of the Gaussians center toward longer
523 wavelengths is obtained in general agreement with the literature (Adams, 1974; Hazen et al., 1978;
524 Cloutis and Gaffey, 1991). This effect is particularly pronounced for the 2 µm absorption (Figure 10-A).
525 Moreover, a linearly coupled behavior is found between the 1 and 2 µm Gaussians strength, i.e. when the
526 1 µm absorption gets stronger, the 2 µm one also increases in proportion, as expected. The "1200"
527 Gaussian strength also increases when dealing with high Fe orthopyroxene (Fig. 9-A right).
528 Analysis of various natural pyroxenes spectra (Fig. 10-B) show that compositions close to
529 endmembers (diopside or enstatite, respectively dots 1-2 and 3-4) have absorption centers similar to those
530 found by Adams (1974). For intermediate composition pyroxenes, the case of augite (dot 6) falls well in

the pyroxene general trend while pigeonite (dot 5) may depart a bit from it. It could be the case with a zoned pyroxene, or in the presence of minor elements such as Ti (Cloutis et al., 2002). Pigeonite is frequently exsolved and/or inverted to orthopyroxene and it may result in a complicated mineralogical texture. Such effects are not yet clearly documented in the literature.

The confrontation of our results with Adams (1974) trends shows that our systematic MGM deconvolution returns a reliable piece of information about the pyroxene type. The next step is to assess how precisely the pyroxene chemical composition can be estimated. To do that, we use data from Hazen et al. (1978) and Cloutis and Gaffey (1991) which documented the evolution of the absorption centers as a function of the Ca and Fe content in the pyroxene quadrilateral. RELAB chemical analysis and literature data have been used to plot the pyroxenes (with colored circles) in the four graphs on Figure 11. Red contoured circles correspond to the set of synthetic orthopyroxenes (Klima et al., 2007) while the blue contoured circles are associated with the various natural pyroxenes described in the previous paragraph. Colors within the circles and in the background correspond respectively to the absorption center position obtained by our approach, and to the determinations found by Hazen et al. (Fig. 11 left) and Cloutis and Gaffey (Fig. 11 right). That way, if the MGM result is in agreement with literature data, the color inside the circle must be the same as the surrounding background color. An overall excellent agreement is found in the case of the suite of synthetic orthopyroxenes as the Fe content varies from 0 (En case) to 100% (Fs case). Our results fit both Hazen et al. and Cloutis and Gaffey data. However, for Ca-rich pyroxenes, discrepancies are observed and our results appear to fit better Cloutis and Gaffey values. In particular, band center positions produced for the three clinopyroxene spectra are at variance with Hazen et al. values, both at 1 and 2 µm. As it stands, we can estimate a range of composition for an unknown pyroxene but not determine very accurately its location in the quadrilateral. Interestingly, going back to the case of the diopside shown on Figure 1, band centers positions found by MGM deconvolution are very consistent for the three powder spectra (1.019 and 2.290 µm for spectrum A, 1.016 and 2.294 µm for spectrum B and 1.017 and 2.307 for spectrum C) and for the three rock spectra (1.044 and 2.266 for spectrum 1, 1.043 and 2.298 for spectrum 2 and 1.038 and 2.253 for spectrum 3).

We also test the capability of our approach to deconvolve pyroxenes mixtures spectra. We here used the set from Sunshine and Pieters (1993). Mixture composition evolves progressively between 100% diopside and 100% enstatite, for three grains size ranges (<45µm, 45-75µm and 75-125µm). The results are illustrated with the case of the less than 45 micron particles suite. Our systematic approach, including the seven configurations, has been applied on the complete set. The configuration(s) validated for each mixing case is (are) reported in Table 3, and the band center positions found at 1 and 2 µm (Fig. 12) are compared to the pyroxene trend defined by Adams (1974). As one could expect, endmembers are modeled by the corresponding appropriate configuration, i.e. either the orthopyroxene or clinopyroxene one. In the case of mixtures, different situations may occur depending on the mixture, and the grains size which modifies the strength and width of the absorptions. Indeed, it is noted that an orthopyroxene will mask clinopyroxene absorptions more easily when dealing with large grains size. However, the general rule is that a mineral which is clearly dominant in the mixture (>75%) is detected by its dedicated

configuration. Then in the case of intermediate mixtures, both the two-components and the dominant pyroxene configurations are validated. In this situation, as defined in the section 2.2.4, the two-components mixture has to be considered as the most representative for detecting the minerals in presence. Conversely, one must bear in mind for the sake of interpretation that below a given critical threshold, a mineral in too weak a proportion may not be detected.

Also, a result of note is to highlight the fact that the band center determination from MGM deconvolution is more accurate in the 1 µm domain than in the 2 µm domain. This may be the result of an indirect edge effect on the continuum caused by the spectral truncature at 2600 nm. Consequently, a more reliable estimation of the pyroxene chemical composition in mixtures situations will be returned from the 1 µm Gaussians.

3.2 Olivine-pyroxene mixtures

3.2.1 Olivine, orthopyroxene without / with plagioclase

As described previously, a number of studies dealing with simple mineralogies exist in the literature. However, there is a lack of quantitative assessment that we address here, concerning the MGM ability to model olivine-pyroxene(s) mixtures spectra. For this purpose, a set of spectra dealing with binary mixtures of olivine (Fo_{90}) and low-calcium pyroxene (hypersthene) ranging from (10% Ol, 90% LCP) to (90% Ol, 10% LCP) (referred to as C1AG14, and C1AG17 to C1AG20 in the RELAB collection) has been used first. Then, a dedicated set of spectra (Mustard and Pieters, 1989; Hiroi and Pieters, 1994) with different amount of olivine (Fo_{85-89}), orthopyroxene (En_{85-90}) and plagioclase ($An_{78}Ab_{22}$) has also been analyzed (cf. Table 4). With this approach, the effect on the deconvolution process of the plagioclase considered as an optically neutral mineral can also be tested.

Our systematic approach, including the seven configurations, has been applied to the complete set. As an example of deconvolution, MGM outputs produced in the case of the Ol50/Opx50 mixture are displayed on Figure 6. The configurations kept for each spectrum are reported in Table 4. First, our approach is tested on a pure plagioclase spectrum. Results show logically that no solution among the seven mafic configurations is validated. For all other spectra, the only validated configurations involve either olivine, orthopyroxene or both minerals. First binary mixtures, involving plagioclase and a mafic mineral are considered. Whatever the abundance of plagioclase, the configuration which is validated corresponds to the proper monomineral one (olivine or orthopyroxene), showing that in these situations the MGM deconvolution is not hampered or biaised by the presence of an optically neutral mineral. This point will be confirmed in the following in the case of ternary mixtures, involving both olivine and orthopyroxene.

Then, Table 4 shows the results when considering ternary mixtures (binary mixtures of olivine and orthopyroxene, with a variable amount of plagioclase). Depending on the olivine/orthopyroxene content, three situations are encountered. First, when orthopyroxene is the dominant mineral (more than 72%

relative to olivine), only its configuration is kept which means that in this context the presence of olivine may not be detected, even if the global shape of the spectra is slightly modified. In fact, the "1200" Gaussian center may be shifted to longer wavelengths, which can be used as an indicator of the olivine presence (Parente and Bishop, 2006). A second situation is found when olivine and orthopyroxene are in the same proportion. Then, two configurations are kept: the orthopyroxene one and the olivine-orthopyroxene mixture one, even with only 16% of each mineral in the mixture composition. As explained earlier (see section 2.2.3 and Fig. 6), the most realistic detection is then provided by the most complex configuration (see Fig. 6). Finally, if olivine represents more than 72% relative to orthopyroxene, only the mixture configuration is validated. We verify here that when the olivine or orthopyroxene is the respective dominant mineral, their absorption bands do not play a symmetrical role (i.e., for Opx/Ol > 72%, orthopyroxene configuration is found while for Ol/Opx > 72%, olivine-orthopyroxene configuration is found) as it was recognized long ago (e.g., Singer, 1981). In conclusion, considering the detection capability of our approach, we note that the presence of olivine can be detected, even when this mineral is not clearly dominant in the mixture. Conversely, this test also shows that some care must be put in the interpretation as when a mineral is not detected, it does not necessarily mean that it is not present in the mixture.

Based on those detections, Gaussians parameters can be used to derive the minerals chemical composition in the case of mafic mineralogies. However, to correctly interpret the centers positions, verification is needed to assess their stability as a function of the minerals content in the case of complex mixtures.

Concerning the band center position of the orthopyroxene Gaussians, the deconvolution process is logically not affected at 2 µm by the presence of olivine, whatever its proportion (Fig. 13). The orthopyroxene 1 µm band center position appears also very stable as long as the olivine relative proportion is less than 70% in the mixture (Fig. 13). The most critical cases arise when the proportion of Opx is low versus Ol+plagioclase (cases of RELAB C1XT32, C1XT 33, C1XT 38). A moderate shift to longer wavelengths on the order of 30 nm is then observed. It suggests that a plagioclase absorption should then be considered in the present MGM modeling and this limitation must be kept in mind for the matter of interpretation.

Then, considering the "850", "1050" and "1250" olivine Gaussians, they present band center positions which are well determined, for olivine proportions exceeding 50%, and are consistent with the respective Fo_{85-90} and Fo_{90} compositions of the samples used here. For lesser proportions, the "1050" appears shifted to longer wavelength and is thus not well determined. In these cases, the 'OPX' configuration is also validated by the MGM modeling, consistent with the fact that in the case of minor proportions of olivine, its detection may be difficult. Though not perfect, these results show that an olivine-pyroxene MGM deconvolution is operational with our approach, and that at least a first-order assessment of the olivine type (i.e. forsterite, fayalite or intermediate compositions) is possible, not excluding a more quantitative estimate in terms of olivine composition.

3.2.2 The most complicated case: an example of ternary mixture of mafic minerals

The case addressed here consists in a mafic ternary mixture (i.e. olivine, orthopyroxene and clinopyroxene). We consider three spectra of the same composition (20% olivine, 20% orthopyroxene and 60% clinopyroxene; RELAB C1XS01, C1XS02, C1XS03) (Mustard et al., 1993; Pieters et al., 1993), referred to as A, B, C in the following. Each mineralogical phase has been separated in three grain sizes (S < 25 µm, M between 25 and 75 µm, L between 75 and 250 µm) and three soils have been created: SS (65% S, 25% M, 10% L), MS (25% S, 50% M, 25% L) and LS (10% S, 25% M, 65% L). Details on spectra A, B, C and RELAB references can be found in Table 5.

The seven configurations, automatically initialized, have been applied on these three spectra and the results are given in Table 5 and figures 14, 15. It is found that four configurations can provide a realistic modeling. However, despite the fact that the CPX configuration is capturing most of the essence of the first-order spectral characteristics (see Fig. 14-A), the successive configurations: 'CPX-OPX', 'CPX-OL', and 'CPX-OPX-OL' improve increasingly the modeling as shown by the rms residuals (0.005 down to 0.0025). As noted earlier, the most complex configuration provides the best description in terms of minerals detection. Interestingly, while it is not the case with the 'CPX-OPX' configuration, the Normalized Band Strength Ratio (NBSR) introduced by Kanner et al. (2007) returns consistent values both at 1 and 2 µm in the case of the'CPX-OPX-OL' configuration.

Those tests on ternary mixtures are not yet complete and beyond this first exploration, a more extensive study remains to be carried out. However, with this new procedure, modeling of complex spectra is no longer out of reach, and the handling of weak spectral signatures requiring an increasing number of Gaussians appear tractable.

4. Conclusion

Our work shows that this new MGM approach is able to model simple and complex mafic mineralogies,including binary and ternary mixtures, for a large range of grain sizes. A key issue is to initialize the MGM procedure with a proper setting for the Gaussians parameters, relying on an automatic analysis of the shape of the spectrum and on the basis of laboratory results available in the literature in the case of simple mixtures of mafic minerals. The continuum is then handled with a second order polynomial adjusted on the local maxima along the spectrum and permits us to address the case of laboratory (controlled powders) and natural rock spectra. The procedure implemented here considers all the mixture possibilities involving orthopyroxene, spectral type B clinopyroxene and olivine and use accordingly for each configuration different numbers of Gaussians, depending on the potential complexity of the mixture. This systematic search is quite efficient to deal with an a priori unknown mafic mineralogy observed in the visible-near infrared by reflectance spectroscopy, as it is frequently the case with hyperspectral orbital data sets.

The results presented in this paper are a quantitative step forward to characterize both modal and chemical compositions of pyroxenes and olivines. A demonstration of the methodology on specific

examples of binary and ternary olivine-pyroxenes mixtures (with and without plagioclase) has been made, which shows that the different non-linear effects which affect the Gaussian parameters (center and strength) can be successfully handled. Of note is the fact that the band center positions associated with the different mafic minerals are not predetermined here in the inverse problem, and thus the MGM outputs are truly informative of the chemical composition of pyroxenes and olivines, keeping in mind that large grains size forsterites have absorption characteristics that may mimic fayalite absorption features. With the consideration of some limits on the detection thresholds, these results are quite promising for increasing the operational use of the Modified Gaussian Model with large hyperspectral data sets, for establishing detailed lithological/mineralogical mappings intended to explore the petrology and geological history of magmatic units (e.g., Bibring et al., 2006; Mustard et al. 2005; Baratoux et al., 2007; Mustard et al. 2007; Combe et al., 2008; Poulet et al., 2009b; Clenet et al., 2010; …).. However, to go further in this work, spectra with a wider range of compositions should be studied, including a variety of pyroxenes chemical compositions and olivine-pyroxene(s) mixtures, in order to thoroughly assess the thresholds of detection and limits on the components quantification. Ultimately, building on the present learning, the use of mineralogical constraints bearing for instance on the coupling of the 1 and 2 micron pyroxene absorptions or on the olivine absorptions, should be set in the correlation matrix to be directly accounted for in the process of the inversion.

Acknowledgments

This project was supported by the French Space Agency CNES and PNP (Programme National de Planétologie) and has benefited from the scientific environment of Paul Sabatier University (Toulouse). Harold Clenet has also benefited of a Ph.D. grant funded by the French ministry of education. Financial and technical support was provided by the Centre National de la Recherche Scientifique (France). We thank R. Klima and E. Cloutis whose thorough comments and suggestions contributed to improve the manuscript. We also deeply acknowledge the support of the RELAB facility and the access to RELAB data.

709 References

710

711 Adams, J. B., 1974. Visible and near IR diffuse reflectance spectra of pyroxenes as applied to remote sensing of solid objects
712 in the solar system. J. Geophys. Res. 79, 4829–4836

713

714 Adams, J. B., 1975. Interpretation of visible and near-infrared diffuse reflectance spectra of pyroxenes and other rock forming
715 minerals. In: Karr, C. (Ed.), Infrared and Raman spectroscopy of lunar and terrestrial materials, New York Academic Press, pp.
716 91–116

717

718 Bibring, J.-P., Langevin, Y., Mustard, J.F., Poulet, F., Arvidson, R.E., Gendrin, A., Gondet, B., Mangold, N., Pinet, P., Forget,
719 F., 2006. Global Mineralogical and Aqueous Mars History Derived from OMEGA/Mars Express Data. Science 312, 400-404
720

721 Baratoux, D., Pinet, P., Gendrin, A., Kanner, L., Mustard, J., Daydou, Y., Vaucher, J. and Bibring, J.-P., 2007. Mineralogical
722 structure of the subsurface of Syrtis Major from OMEGA observations of lobate ejecta blankets. J. Geophys. Res. 112, E08S05

723

724 Bishop, J.L., Pieters, C.M., Hiroi, T., Mustard, J.F.,1998. Spectroscopic analysis of Martian meteorite ALH 84001 powder and
725 applications for spectral identification of minerals and other soil components on Mars. Meteorit. Planet. Sci. 33, 699–708

726

727 Burns, R.G., 1970. Crystal field spectra and evidence of cation ordering in olivine minerals. Am. Mineral. 55, 1608–1632

728

729 Burns, R. G., 1993. Mineralogical applications of crystal field theory, second ed. Cambridge Univ. Press, Cambridge, UK. 551
730 pp.

731

732 Clark, R. N. and Roush, T. L., 1984. Reflectance spectroscopy: Quantitative analysis techniques for remote sensing
733 applications. J. Geophys. Res. 89(B7), 6329–6340

734

735 Clark, R. N., Swayze, G. A., Livo, K. E., Kokaly, R. F., Sutley, S. J., Dalton, J. B., McDougal, R. R. and Gent, C. A., 2003.
736 Imaging spectroscopy: Earth and planetary remote sensing with the USGS Tetracorder and expert systems. J. Geophys. Res.
737 108(E12), 5131

738

739 Clenet, H., Pinet, P. C., Daydou, Y. D., Heuripeau, F., Rosemberg, C., Ceuleneer, G., 2008. A Systematic Testing Approach
740 Using the Modified Gaussian Model (MGM) for Mafic Mineralogy Mapping in Natural Conditions (Earth, Mars), Lunar
741 Planet. Sci. 39th, p.1918 (abstract 1391)

742

743 Clenet, H., 2009. Télédétection hyperspectrale : minéralogie et pétrologie, Application au volcan Syrtis Major (Mars) et à
744 l'ophiolite d'Oman. Thesis, Toulouse University, Toulouse. 362 pp.

745

746 Clenet, H., Ceuleneer, G., Pinet, P., Abily, B., Daydou, Y., Harris, E. and C. Dantas, 2010. Thick sections of layered ultramafic
747 cumulates in the Oman ophiolite revealed by an airborne hyperspectral survey: petrogenesis and relationship to mantle
748 diapirism, Lithos 114(3-4),265-281

749

750 Cloutis, E.A., Gaffey, M.J.,. Jackowski, T.L, Reed, K.L., 1986. Calibrations of phase abundance, composition, and particle size
751 distribution for olivine-orthopyroxene mixtures from reflectance spectra. J. Geophys. Res. 91(B11), 11,641–11,653

752

753 Cloutis, E.A., Gaffey, M.J., 1991. Pyroxene spectroscopy revisited: Spectral-compositional correlations and relationship to
754 geothermometry. J. Geophys. Res. 96(E5), 22,809–22,826
755
756 Cloutis, E. A., 2002. Pyroxene reflectance spectra: Minor absorption bands and effects of elemental substitutions. J. Geophys.
757 Res. 107, NO. E6, 5039
758
759
760 Combe, J.P., Launeau, P., Pinet, P.C., Despan, D., Harris, E., Ceuleneer, G., Sotin, C.,2006. Mapping of an ophiolite complex
761 by high resolution visible-infrared spectrometry, *Geochem. Geophys. Geosyst., 7, Q08001*
762
763 Combe, J.-P., Le Mouélic, S., Sotin, C., Gendrin, A., Mustard, J.F., Le Deit, L., Launeau, P., Bibring, J.-P., Gondet, B.,
764 Langevin, Y., Pinet, P. and the OMEGA Science Team, 2008. Analysis of OMEGA/Mars Express data hyperspectral data
765 using a Multiple-Endmember Linear Spectral Unmixing Model (MELSUM): Methodology and first results. Planet. Space Sci.
766 56, 951-975
767
768 Crown, D.A., Pieters, C.M., 1987. Spectral properties of plagioclase and pyroxene mixtures and the interpretation of lunar soil
769 spectra. Icarus 72, 492-506
770
771 Harloff, J., Arnold, G., 2001. Near-infrared reflectance spectroscopy of bulk analog materials for planetary crust. Planet. Space
772 Sci. 49, 191-211
773
774 Hazen, R.M., Bell, P.M., Mao, H.K., 1978. Effects of compositional variation on absorption spectra of lunar pyroxenes. Proc.
775 Lunar Sci. Conf. 9, 2919–2934
776
777 Hiroi, T., C. M. Pieters, 1994. Estimation of grain sizes and mixing ratios of fine powder mixtures of common geologic
778 minerals. J. Geophys. Res. 99, 10867–10879
779
780 Hunt, G. R., Salisbury, J.W., 1970. Visible and near infrared spectra of minerals and rocks, I, silicate minerals. Mod. Geol. 1,
781 283–300
782
783 Hunt, G. R., 1977. Spectral signatures of particulate minerals in the visible and near infrared. Geophysics 42, 501–513
784
785 Kanner, L.C., Mustard, J.F., Gendrin, A., 2007. Assessing the limits of the Modified Gaussian Model for remote spectroscopic
786 studies of pyroxenes on Mars. Icarus 187, 442–456
787
788 King, T.V., Ridley, W.I., 1987. Relation of the spectroscopic reflectance of olivine to mineral chemistry and some remote
789 sensing implications. J. Geophys. Res. 92, 11,457–11,469
790
791 Klima, R.L., Pieters, C.M., Dyar, M., 2007. Spectroscopy of synthetic Mg-Fe pyroxenes I: Spin-allowed and spin-forbidden
792 crystal field bands in the visible and near-infrared. Meteorit. Planet. Sci. 42, 235–253
793
794 Lucey, P. G., 1998. Model near-infrared optical constants of olivine and pyroxene as a function of iron content. J. Geophys.
795 Res. 103, 1703-1713
796

McCord, T.B., Clark, R.N. Hawke, B.R., McFadden, L.A., Owensby P.D., Pieters, C.M., Adams J.B., 1981. Moon' Near-Infrared Spectral Reflectance, A First Good Look. J. Geophys. Res. 86, 10,883-10,892

Mustard, J.F., Pieters, C.M., 1989. Photometric phase functions of common geologic minerals and applications to quantitative analysis of mineral mixture reflectance spectra. J. Geophys. Res. 94, 13,619–13,634

Mustard, J.F., Sunshine, J.M., Pieters, C.M., Hoppin, A., Pratt, S.F., 1993. From minerals to rocks: Toward modeling lithologies with remote sensing. Lunar Planet. Sci. XXIV, 1041-1042 (abstract)

Mustard, J.F., Sunshine, J.M., 1995. Seeing through the dust: Martian crustal heterogeneity and links to the SNC meteorites. Science 267, 1623–1626

Mustard, J.F., Hays, J.E., 1997. Effects of hyperfine particles on reflectance spectra from 0.3 to 2.5 µm. Icarus 125, 145-163

Mustard, J.F., Murchie, S., Erard, S., Sunshine, J., 1997. In situ compositions of Martian volcanics: Implications for the mantle. J. Geophys. Res. 102, 25,605–25,615

Mustard, J.F., Poulet, F., Gendrin, A., Bibring, J.-P., Langevin, Y., Gondet, B., Mangold, N., Bellucci, G., Altieri, F., 2005. Olivine and pyroxene diversity in the crust of Mars, Science, 307, 1594-1597.

Mustard, J.F., Poulet, F., Head, J.W., Mangold, N., Bibring, J.-P., Pelkey, S.M., Fassett, C.I., Langevin, Y., Neukum, G., 2007. Mineralogy of the Nili Fossae region with OMEGA/Mars Express data: 1. Ancient impact melt in the Isidis Basin and implications for the transition from the Noachian to Hesperian. J. Geophys. Res. 112, E08S03

Noble, S.K., Pieters, C.M., Hiroi, T.,Taylor, L.A., 2006. Using the modified Gaussian model to extract quantitative data from lunar soils. J. Geophys. Res. 111, E11009

Parente, M., Bishop, J.L., 2006. Deconvolution of reflectance spectra using nonlinear least squares curve fitting: application to martian meteorites. Lunar Planet. Sci. 37, Abstract 1537

Pieters, C.M., 1983. Strength of mineral absorption features in the transmitted component of near-infrared reflected light: First results from RELAB. J. Geophys. Res. 88, 9534–9544

Pieters, C.M., Mustard, J.F., Pratt, S.F, Sunshine, J.M., Hoppin, A., 1993. Visible-infrared properties of controlled laboratory soils. Lunar Planet. Sci. XXIV, 1147-1148 (abstract)

Pieters, C.M., Hiroi, T., 2004. RELAB (Reflectance Experiment Laboratory): A NASA multiuser spectroscopy facility. Lunar Planet. Sci. 35 , Abstract 1720

Pinet, P.C., Clenet, H., Rosemberg, C., Ceuleneer, G., Heuripeau, F., Harris, E., Daydou, Y., Baratoux, D., Chevrel, S., Launeau, P., Combes, J.-P., LeMouélic, S., Sotin, C., 2006. Mantle Rock Surface Mineralogy Mapping in Arid Environment From Imaging Spectroscopy: The Case Of The Maqsad Peridotitic Massif In Oman And Implications For The Spectroscopic Study Of Exposed Mafic Units On Mars. Lunar Planet. Sci., Abstract 1346

Pinet, P.C., Heuripeau, F., Clenet, H., Chevrel, S., Daydou, Y., Baratoux, D., Rosemberg, C., Bibring, J.-P., Poulet, F., Gondet, B., Mustard, J., LeMouélic, S., Bellucci, G., and the OMEGA team, 2007. Mafic Mineralogy Variations Across Syrtis Major Shield And Surroundings As Inferred From Visible-Near-Infrared Spectroscopy By Omega/Mars Express. Mars Conf. 7, Pasadena, Abstract 3146.

Pinet, P.C., Clenet, H., Heuripeau, F., Chevrel, S. D., Rosemberg, C., Daydou, Y., Toplis, M., Baratoux, D., 2009. Mafic Mineralogy of Martian Meteorites Based on a Systematic Deconvolution Using an Improved Modified Gaussian Model (MGM) Approach. Lunar Planet. Sci., Abstract 1612

Pompilio, L., Roush, T.L., Pedrazzi, G., Sgavetti, M., 2006. VNIR spectral modeling of Mars analogue rocks: first results. 1st Europlanet Conf., Berlin

Pompilio, L., Sgavetti, M., Pedrazzi, G., 2007. Visible and near-infrared reflectance spectroscopy of pyroxene-bearing rocks: New constraints for understanding planetary surface compositions. J. Geophys. Res. 112, E01004

Pompilio, L., Pedrazzi,G, Sgavetti, M, Cloutis, E.A,. Craig, M.A., Roush, T.L., 2009. Exponential Gaussian approach for spectral modeling: The EGO algorithm I. Band saturation. Icarus 201, 781–794

Poulet, F., Bibring, J.-P., Langevin, Y., Mustard, J.F., Mangold, N., Vincendon, M., Gondet, B., Pinet, P., Bardintzeff, J.-M., Platevoet, B, 2009a. Quantitative compositional analysis of Martian mafic regions using MEx/OMEGA reflectance data: 1. Methodology, uncertainties and examples of application. Icarus 201, 69-83

Poulet, F., Mangold, N., Platevoet, B., Bardintzeff, J.-M., Sautter, V., Mustard, J.F., Bibring, J.-P., Pinet, P., Langevin, Y., Gondet, B., Aléon-Toppani, A., 2009b. Quantitative compositional analysis of martian mafic regions using the MEx/OMEGA reflectance data: 2. Petrological implications. Icarus, 201, 84-101.

Roy, R., Launeau, P., Carrère, V., Pinet, P., Ceuleneer, G., Clenet, H., Daydou, Y., Girardeau, J., Amri, I., 2009. Geological mapping strategy using VNIR hyperspectral remote sensing: application to the Oman ophiolite (Sumail Massif). Geochem. Geophys. Geosyst. 10, Q02004

Schade, U., Wäsch, R., Moroz, L., 2004. Near-infrared reflectance spectroscopy of Ca-rich clinopyroxenes and prospects for remote spectral characterization of planetary surfaces. Icarus 168, 80-92

Singer, R.B., 1981. Near-infrared spectral reflectance of mineral mixtures: Systematic combinations of pyroxenes, olivine and iron oxides. J. Geophys. Res. 86, 7967–7982

Sunshine, J.M., Pieters, C.M., Pratt, S.F., 1990. Deconvolution of mineral absorption bands: an improved approach. J. Geophys. Res. 93, 6955–6966

Sunshine, J.M., Pieters, C.M., 1993. Estimating modal abundances from the spectra of natural and laboratory pyroxene mixtures using the modified Gaussian model. J. Geophys. Res. 98, 9075–9087

Sunshine, J.M., Pieters, C.M., 1998. Determining the composition of olivine from reflectance spectroscopy. J. Geophys. Res. 103, 13,675-13,688

886 Sunshine, J.M., Pieters, C.M., Pratt, S.F., McNaron-Brown, K.S., 1999. Absorption band modeling in reflectance spectra:
887 availability of the Modified Gaussian Model. Lunar Planet. Sci. 30, Abstract 1306
888
889 Tarantola, A., Valette, B., 1982. Generalized nonlinear inverse problems solved using the least squares criterion. Rev.
890 Geophys. Space Phys. 20, 219–232
891

Figures captions

Tab. 1

Gaussians present in the different configurations, with Ol for olivine, Opx for orthopyroxene and Cpx for clinopyroxene (spectral type B). Gaussians are named by the position of their center. An "X" means that the Gaussian is used in the corresponding configuration.

Tab. 2

Suite of 28 olivine spectra used, spanning the whole range of composition from $Fo_{0.1}$ to $Fo_{96.9}$, with variable grain sizes. Rms estimates indicate the quality of the spectral fit obtained with the olivine configuration.

Tab. 3

Summary of the retained configurations as a function of the relative abundance of diopside and enstatite in the mixture. Endmembers are modeled with one configuration only while mixtures can be correctly modeled with one or two configurations. As explained previously in the text, when two configurations are validated the most complex one should be used to extract chemical compositions (see text for details). Rms estimates indicate the quality of the spectral fit.

Tab. 4

Summary of the retained configurations as a function of the abundance of olivine, orthopyroxene and plagioclase in the mixture (grains size: 45-75µm). Rms estimates indicate the quality of the spectral fit.

Tab. 5

Summary of the performances associated with each configuration for the three investigated spectra involving a ternary mafic mixture (Opx, Cpx, Ol). Rms estimates indicate the quality of the spectral fit associated with the retained configuration(s).

Fig. 1

Differences between powder spectra (labeled A (0<Ø<45µm), B (45<Ø<75µm), C (75<Ø<125µm)) acquired in laboratory (dashed lines) and natural rocks spectra (labeled 1, 2, 3) we acquired during a field campaign in Oman with an ASD FieldSpec® (plain lines). All the spectra correspond to clinopyroxene (diopside: powder $Wo_{46}En_{46}Fs_{9}$; rock: $Wo_{48}En_{47}Fs_{5}$) with almost the same chemical composition (RELAB database and microprobe analysis). One can see that field spectra show less pronounced absorption bands and a lower reflectance mean level.

Fig. 2

Parameters used to define a spectrum global shape. In this example, the spectrum is an olivine-orthopyroxene mixture (respectively 75% and 25%) from the RELAB spectral library.

Fig. 3

a) Variations of the absorptions strengths simulated by an artificial flattening of a laboratory spectrum (mixture of 40% Opx and 60% Cpx). 0% corresponds to the reference spectrum from RELAB library. Absorptions characteristics are modulated from 0 to 100%, i.e. a perfectly flat spectrum. b) Final center of the orthopyroxene gaussians (color [or grey] scale) as a function of the initialization strength (horizontal axis) and the flattening of the spectrum (vertical axis). Dashed lines defined an area corresponding to the values given by Sunshine and Pieters (1993), taking into account for the variability defined by Kanner et al. (2007). c) Final strength of the orthopyroxene gaussians (color [or grey] scale) as a function of the initialization strength (horizontal axis) and the flattening of the spectrum (vertical axis).

Fig. 4

Relations between parameters defined in Fig. 2; mixture characteristics and Gaussians parameters as calculated by Sunshine et al. (1993) for this set. We use spectra from the RELAB library, considering a two-pyroxene mixture (100% clinopyroxene to 100% orthopyroxene) with three grain size (<45µm (displayed with black dots), between 45 and 75µm (displayed with dark grey dots) and between 75 and 125µm (displayed with light grey dots)). Diagram a: Ratio between the Gaussians strength of the two pyroxenes calculated by Sunshine et al. and the mixture composition, estimated from the first step of our approach (see text); Diagram b: relation between the Gaussians strength of a given pyroxene (opx or cpx) at 1 and 2 micron as a function of the orthopyroxene proportion in the mixture composition (black square corresponds to 1 micron opx band strength, black star to 2 micron opx band strength, grey square to 1 micron cpx band strength, grey star to 2 micron cpx band strength, black triangle to the ratio of the 1µm opx band strength/ 2µm opx band strength (opx_1/opx_2), grey triangle to the ratio of the 1µm cpx band strength/ 2µm cpx band strength (cpx_1/cpx_2)). In both diagrams, five intervals separated by vertical dashed lines are defined as a function of the mixture composition. For each interval, empirical coefficients have been defined (see text) (e.g., in diagram a, Cpx strength/Opx strength ratio is successively equal to 2/1, 1/1,1/2, 1/12, 1/12; in diagram b, opx_1/opx_2 is equal to 1.7, 1.5, 1.5, 1.4, 1.35 and cpx_1/cpx_2 .is equal to 3.08, 2.92, 2.76, 2.58, 2.45). The two hatched black and grey lines visualize the result of the linear regressions for opx and cpx, respectively.

Fig. 5

Calculated Gaussians parameters obtained with the automatic initialization. Tests with synthetic spectra are similar to the tests described in Fig. 3. Pyroxenes mixture results are represented on the left side while olivine-orthopyroxene mixture results are represented on the right side. From top to bottom, parameters considered are the band center positions, strengths for all the Gaussians.

Fig. 6

MGM Analysis of a 50/50 olivine-orthopyroxene mixture spectrum (RELAB C1XT31). Shown on each graph are the measured spectrum, the spectral position of the local maxima along the spectrum used for the process of initialization (see section 2.2), the MGM modeled spectrum with the Gaussians and polynomial determined by the MGM deconvolution and the residuals line along the spectral domain. Gaussians are displayed with a solid black line for orthopyroxene and a dotted grey line for olivine. Solid grey line corresponds to Gaussian "1200". Hatched line corresponds to the continuum produced with a second-order polynomial. For the sake of clarity, the residuals (observed – modeled quantity) are shifted by +0.1 which means that a perfect fit, with a zero residual value all along the spectral domain, is displayed with a flat line with a 0.1 ordinate. Two solutions are retained. Fig. 6a. 'OPX' configuration (rms = 0.014). Fig. 6b. 'OL-OPX' configuration (rms=0.006 and the residuals line is clearly smoother along the spectrum). The 'OL-OPX' configuration delivers the best modeling.

Fig. 7

Example of results (same display as fig. 6) given by our approach in the case of the olivine configuration, for three different chemical compositions in the solid solution (respectively $Fo_{0,1}$ (RELAB C1PO58 < 45 µm), $Fo_{50.5}$ (RELAB C1PO49 < 45 µm) and $Fo_{96.9}$ (RELAB C1PO52 < 45 µm). Each time the Gaussian functions parameters are in agreement with literature trends.

Fig. 8

Effect of olivine grains size on the spectral shape (left) and corresponding MGM results (right). Olivine (Hawaii) has a fixed chemical composition (forsterite Fo_{88}). Spectra have been measured with an ASD FieldSpec® at our laboratory (DTP/UMR 5562). Large grains size forsterite displays absorption characteristics that may mimic fayalite absorption features. This effect, not really documented in the literature appears when the grains size exceeds 250 µm.

Fig. 9

Example of results (same display as fig. 6) given by our approach in the case of spectra of various pyroxenes showing different chemical compositions. Gaussians are displayed with a hatched-dotted black line for clinopyroxene and a solid black line for orthopyroxene. Solid grey line corresponds to Gaussian "1200". Hatched line corresponds to the continuum produced with a second-order polynomial. Fig. 9a: case of synthetic pyroxenes (Klima et al., 2007): (1) refers to Enstatite ($En_{97}Fs_2$) (RELAB C1DL64A), (2) refers to Ferrosilite (En_0Fs_{100}) endmember (RELAB C1DL61A). Fig. 9b: case of natural pyroxenes (pigeonite $Wo_8En_{65}Fs_{27}$ (RELAB C1PP42) and augite $Wo_{39}En_{42}Fs_{19}$ (RELAB C1PP49)). Orthopyroxene configuration is kept in the case of enstatite, ferrosilite and pigeonite while clinopyroxene configuration is kept for augite. Gaussian functions parameters are in agreement with literature trends.

Fig. 10

Evolution of MGM calculated centers at 1 and 2 µm compared to pyroxenes trend defined by Adams (1974). Left (Fig. 10a): in the case of a synthetic orthopyroxene set (Klima et al., 2007) ranging from enstatite (En_0Fs_{100}) to ferrosilite ($En_{97}Fs_2$). Right (Fig. 10b): examples of various pyroxenes coming from the RELAB library (compositions are respectively: (1) diopside $Wo_{49}En_{43}Fs_8$ (C1PP29), (2) diopside $Wo_{45}En_{45}Fs_{10}$ (C5PP21),(3) enstatite $Wo_1En_{91}Fs_8$, (C1PP43), (4) enstatite $Wo_1En_{87}Fs_{12,}$ (C5PE30), (5) pigeonite $Wo_8En_{65}Fs_{27}$ (C1PP42) and (6) augite $Wo_{39}En_{42}Fs_{19}$ (C1PP49),). Error bars correspond to uncertainties from Kanner et al. (2007), i.e. ±8 nm in the 1 µm domain and ±17 nm in the 2 µm domain. Pyroxenes 2 and 4, are the two pyroxene endmembers used in the case of diopside/enstatite mixtures from Sunshine and Pieters (1993). The present MGM results agree with Adams (1974) except for the case of pigeonite which appears slightly off trend.

Fig. 11

Chemical compositions estimated from Gaussian centers parameters. Left: data from Hazen et al. (1978); Right: data from Cloutis and Gaffey (1991). Pyroxenes used are those described in Figure 10. In the four quadrilaterals, each circle indicates the true chemical composition of the corresponding pyroxene (data from RELAB). Colors within the circles and in the background correspond respectively to the absorption center position at 1 and 2 µm obtained by our approach, and to the determinations found by Hazen et al. and Cloutis and Gaffey. That way, if the MGM result is in agreement with literature data, the color inside the circle must be the same as the surrounding background color,

Fig. 12

MGM calculated centers at 1 and 2 µm compared to pyroxenes trend defined by Adams (1974) in the case of diopside/enstatite mixture (<45 µm micron particles suite) from Sunshine and Pieters (1993). The two minerals have a fixed chemical composition and only their relative abundance varies (i.e. Gaussian centers should be always the same as 2 and 4 in Fig. 9). Bold crosses correspond to the center band positions found with MGM deconvolution by Sunshine and Pieters (1993) for the pyroxene end-member spectrum (respectively, 0.91, 1.83 µm for opx, and 1.01, 2.27 µm for cpx mineral. Symbols (cross, triangle, losange) indicate the MGM configuration used in the present approach, respectively 'OPX',' CPX', 'CPX-OPX'. Figures mentioned within the symbols indicate the proportion of clinopyroxene in the mixture. Concerning the opx detection, one notes that for both 'OPX' and'CPX-OPX' configurations the result for the opx 1 µm band center positions is extremely stable whatever the mixture while a progressive shift is seen for the opx 2 µm band center position when the cpx mineral prevails in the mixture (60, 75, 85%). Concerning the cpx detection, for both 'CPX' and 'CPX-OPX' configurations, the 1 µm band center position is well determined whatever the mixture while some scattering on the order of 30-40 nm is observed with the 2 µm band center position. For high cpx proportions (75, 85, 100%), the'CPX'configuration returns very close solutions (within 10 nm) compared to the reference case.

Fig. 13

Band center position of orthopyroxene Gaussians at 1 and 2 µm and olivine Gaussians at 0.85, 1.05 and 1.2 µm from MGM deconvolution for olivine-pyroxene(s) mixtures spectra. A set of spectra with binary mixtures of olivine (Fo_{90}) (referred to as endmember Fo_1) and low-calcium pyroxene (hypersthene) (referred to as endmember En_1) ranging from (10%Ol, 90%LCP) to (90%Ol, 10%LCP) (referred to as C1AG14, and C1AG17 to C1AG20 in the RELAB collection) has been used first. MGM results are displayed by means of losange symbol.

Then, a dedicated set of spectra with different amount of olivine (Fo_{85-89}) (referred to as endmember Fo_2), orthopyroxene (En_{85-90}) (referred to as endmember En_2) and plagioclase ($An_{78}Ab_{22}$) has also been analyzed. MGM results are displayed by means of triangle symbol. Open symbols (losange and triangle) refer to the use of monomineral configurations, either 'OPX' or 'OL' one. Filled symbols (grey-colored losange and triangle) refer to the use of 'OL-OPX' configuration. Cross symbol refers to the 'OL-OPX-CPX' configuration applied to the spectra with a ternary mixture (ol,opx,cpx) (see also figure 14). Large scale symbols on the 0% vertical axis represent the orthopyroxene bands center for En_1 and En_2 endmembers; shaded large scale symbols on the 100% vertical axis represent the olivine bands center for Fo_1 and Fo_2 endmembers. Small size triangles correspond to En1 mixed with variable plagioclase proportions: results demonstrate the orthopyroxene band center positions are unaffected

Fig. 14

MGM deconvolution (same display as Fig. 6) for the case of a ternary mafic mixture (20% ol, 20% opx, 60% cpx) spectrum from RELAB (C1XS03). Gaussians are displayed with a hatched-dotted black line for clinopyroxene, a solid black line for orthopyroxene and a dotted grey line for olivine. Solid grey lines correspond to Gaussians "650" and "1200". Hatched line corresponds to the continuum produced with a second-order polynomial. Fig. 14A: 'CPX' configuration, Fig. 14B: 'CPX-OPX' configuration, Fig. 14C: 'CPX-OL' configuration, Fig. 14D: 'CPX-OPX-OL' configuration. The band center position for olivine and orthopyroxene Gaussians are displayed with crosses on figure 13 (see Fig. 13).

Fig. 15

MGM analysis of a ternary mafic mixture (20% ol, 20 % opx, 60% cpx) spectrum. Orthopyroxene and clinopyroxene band center positions determined by MGM deconvolution plotted over Adams (1974) representation. Symbols (triangle, star, losange, square) indicate the successive MGM configurations used in the present approach, respectively 'CPX','OL-CPX', 'OPX-CPX', 'OL-OPX-CPX'. Their size reflects the MGM associated uncertainty (on the order of 10-20 nm) on a band center position (Kanner et al., 2007). Letters A, B, C refer to the three spectra used (see text and table 5 for details). Results with A, B, C spectra appear very consistent for each configuration. Clinopyroxene mineral which is dominant is correctly determined with the 'CPX' configuration, in close agreement with the results returned by the 'OL-CPX'configuration. Then, orthopyroxene mineral is consistently detected by both the 'OPX-CPX' and 'OL-OPX-CPX'configurations. While the results for the cpx 1 µm band and the opx 2 µm band

1082 center positions are quite stable whatever the configuration, the opx 1 µm band and the cpx 2 µm band
1083 center positions shift by a few tens of nanometers and are responsible for the observed scattering, which
1084 however does not hamper the detection of the three mafic minerals.
1085
1086
1087

1088 **Table 1**

1089

	OL	OPX	CPX	OL-OPX	OL-CPX	OPX-CPX	OL-OPX-CPX
450	X	X	X	X	X	X	X
650		X	X	X	X	X	X
850	X			X	X		X
900		X		X		X	X
1000			X		X	X	X
1050	X			X	X		X
1200		X	X			X	
1250	X			X	X		X
1800		X		X		X	X
2150			X		X	X	X
Tot. Nb.	4	5	5	7	7	7	9

1090

1091

1092 **Table 2**

1093

Relab spectrum	Fo	Grain size	*rms*
C1PO58	0,1	< 45 µm	0,0040
C3PO59	0,1	45 - 90 µm	0,0070
C1PO48	27,7	< 45 µm	0,0094
C1PO72	36,0	< 45 µm	0,0041
C1PO74	42,0	< 45 µm	0,0038
C1PO49	50,5	< 45 µm	0,0055
C1PO47	59,3	< 45 µm	0,0099
C1PO45	60,0	< 45 µm	0,0098
C1PO30	82,4	< 45 µm	0,0046
C2PO31	82,4	< 45 µm	0,0024
C1OL01	85,0	< 45 µm	0,0044
C2OL08	85,7	< 45 µm	0,0064
C1PO64	85,9	< 45 µm	0,0049
C1PO40	88,0	< 45 µm	0,0049
C3PO57	88,5	> 45 µm	0,0088
C1PO27	89,0	< 45 µm	0,0057
C1OL02	90,0	< 45 µm	0,0068
CAPO50	90,4	< 45 µm	0,0024
C2OL04	90,5	< 45 µm	0,0026
C2OL10	90,8	< 45 µm	0,0052
C1OL03	91,0	< 45 µm	0,0132
C1PO60	91,8	< 45 µm	0,0041
C3PO61	91,8	> 45 µm	0,0067
C1PO76	92,0	< 45 µm	0,0030
C1PO77	92,0	> 45 µm	0,0035
C3PO54	92,7	> 45 µm	0,0406
C1PO52	96,9	< 45 µm	0,0026
C3PO53	96,9	> 45 µm	0,0035

1094

1095

Table 3

Relab spectrum	Mixture composition		Configuration kept (rms)		
	Opx	**Cpx**	**OPX**	**OPX-CPX**	**CPX**
C5PE30	**100%**	0%	0.0041		
C1XP15	85%	15%	0.0039	0.0036	
C1XP13	75%	25%	0.0045	0.0035	
C1XP11	60%	40%	0.0054	0.0031	
C1XP10	50%	50%		0.0027	
C1XP12	40%	60%		0.0027	
C1XP14	25%	75%		0.0027	0.0096
C1XP16	15%	85%		0.0030	0.0083
C5PP21	0%	**100%**			0.0050

Table 4

Relab spectrum	Mixture composition			Relative proportion		Configuration kept (rms)		
	Ol	**Opx**	**Pl**	**Ol**	**Opx**	**OL**	**OPX**	**OL-OPX**
CCPA60	0%	0%	**100%**	0%	0%			
C3PE41	0%	**100%**	0%	0%	100%		0.0185	
C1XT29	0%	75%	25%	0%	100%		0.0148	
C1XT28	0%	50%	50%	0%	100%		0.0132	
C1XT27	0%	25%	75%	0%	100%		0.0131	
CCPO81	**100%**	0%	0%	100%	0%	0.0065		
C1XT24	75%	0%	25%	100%	0%	0.0144		
C1XT25	50%	0%	50%	100%	0%	0.0213		
C1XT26	25%	0%	75%	100%	0%	0.0278		
C1XT34	17%	67%	17%	20%	80%		0.0130	
C1XT30	25%	75%	0%	25%	75%		0.0152	
C1XT37	17%	42%	42%	29%	71%		0.0118	
C1XT31	50%	50%	0%	50%	50%		0.0147	0.0064
C1XT39	42%	42%	17%	50%	50%		0.0139	0.0051
C1XT36	33%	33%	33%	50%	50%		0.0127	0.0053
C1XT35	17%	17%	67%	50%	50%		0.0131	0.0103
C1XT38	42%	17%	42%	71%	29%		0.0125	0.0080
C1XT32	75%	25%	0%	75%	25%			0.0049
C1XT33	67%	17%	17%	80%	20%			0.0057
C1AG09	0%	**100%**	0%	0%	100%		0.0104	
C1AG17	10%	90%	0%	10%	90%		0.0080	0.0042
C1AG18	30%	70%	0%	30%	70%		0.0079	0.0039
C1AG19	50%	50%	0%	50%	50%		0.0074	0.0024
C1AG14	70%	30%	0%	70%	30%		0.0083	0.0023
C1AG20	90%	10%	0%	90%	10%			0.0023
C1AG08	**100%**	0%	0%	100%	0%	0.0036		

Table 5

Relab spectrum	Grain size			Configuration kept (rms)			
	Cpx	**Opx**	**Ol**	**CPX**	**OL-CPX**	**OPX-CPX**	**OL-CPX-OPX**
C1XS01 (A)	MS	MS	MS	0.0065	0.0065	0.0026	0.0024
C1XS03 (B)	LS	LS	SS	0.0050	0.0047	0.0028	0.0025
C1XS02 (C)	SS	SS	LS	0.0060	0.0056	0.0026	0.0026

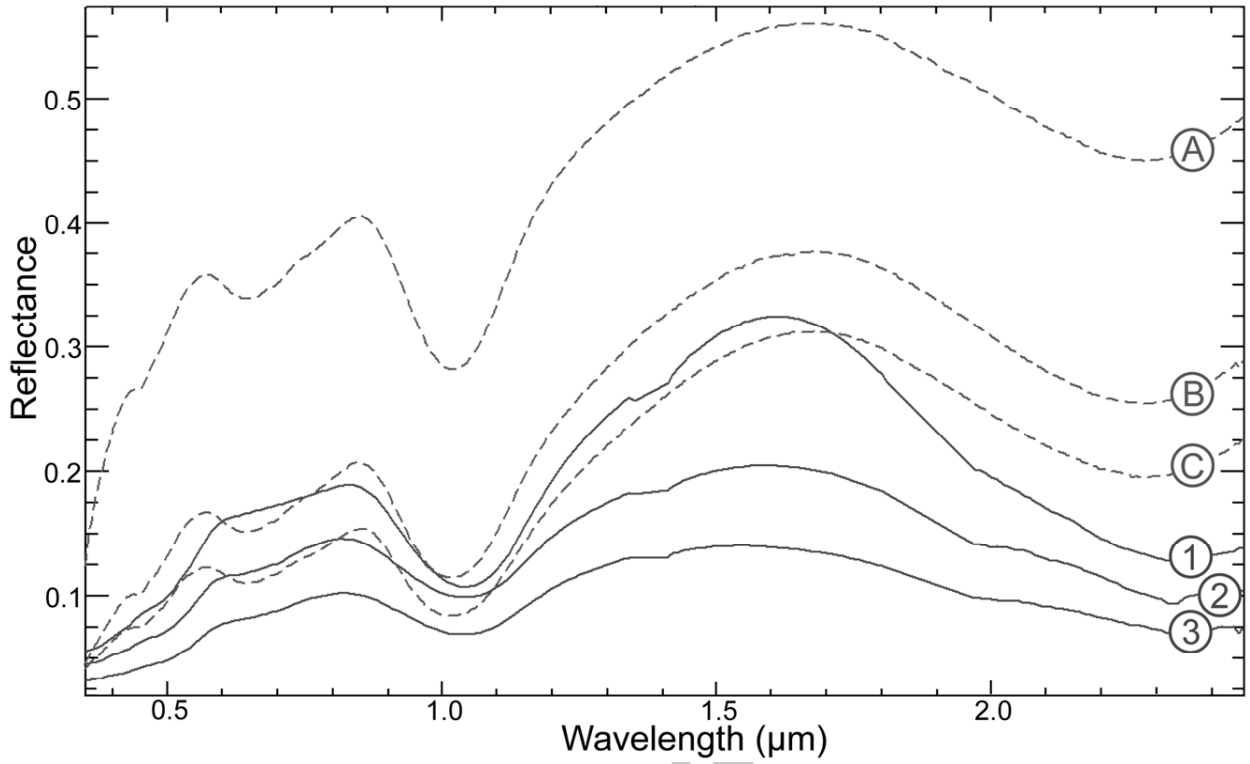

Figure 1

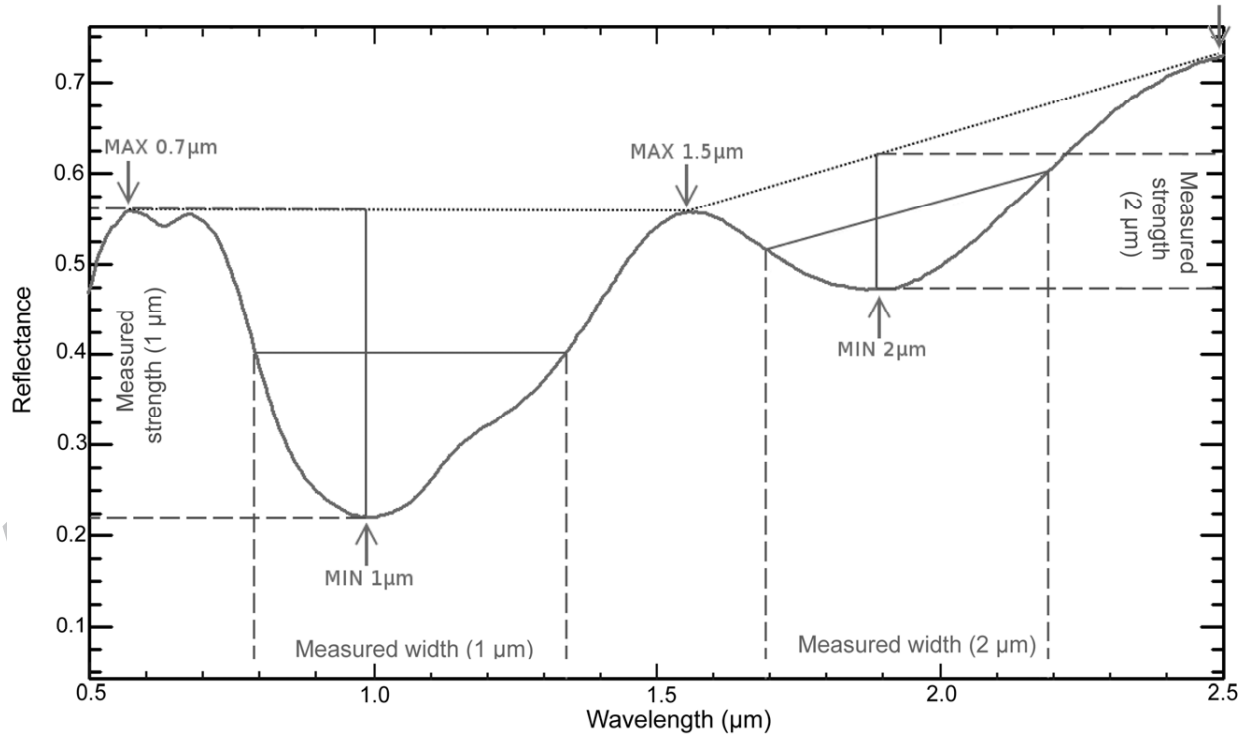

Figure 2

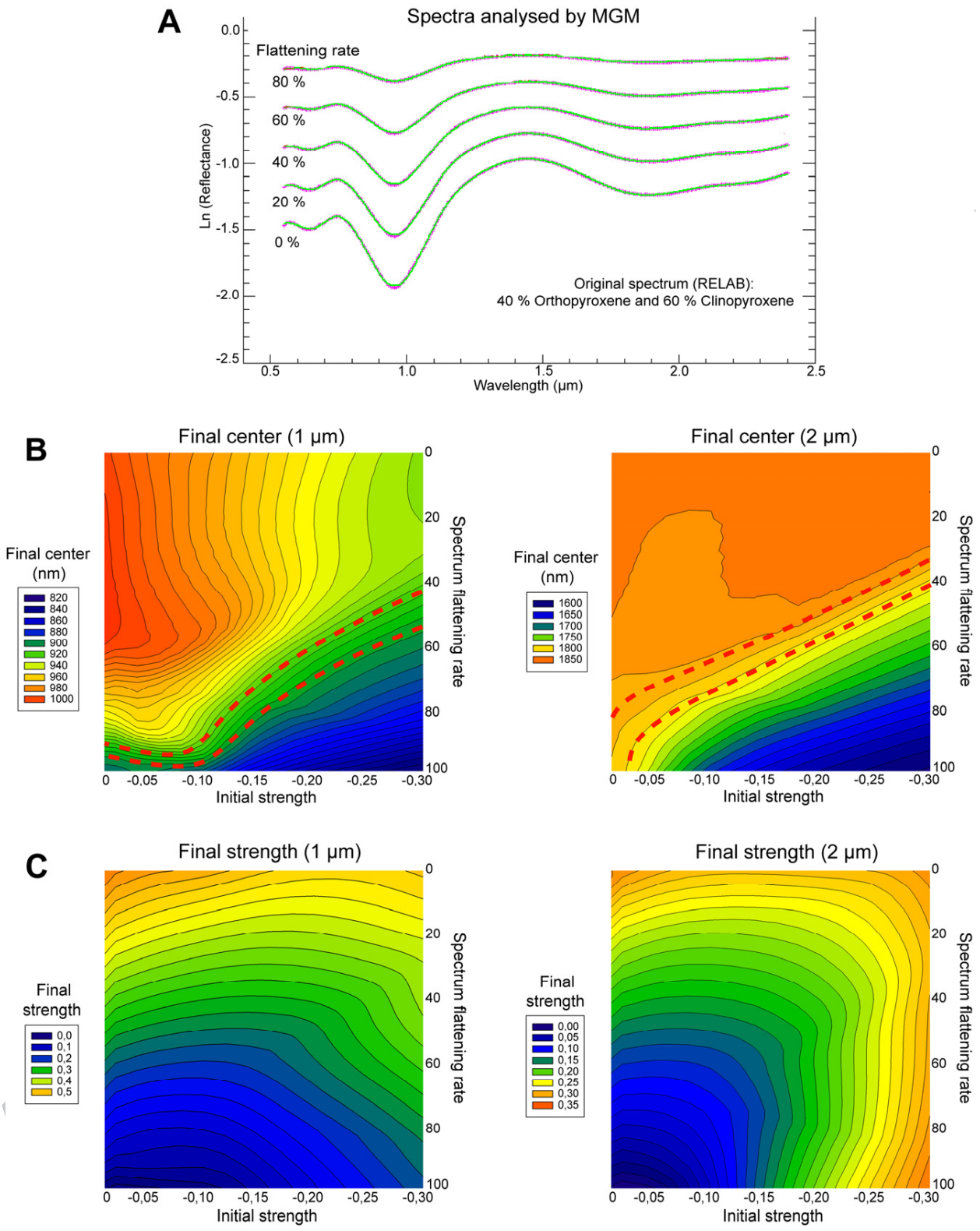

Figure 3

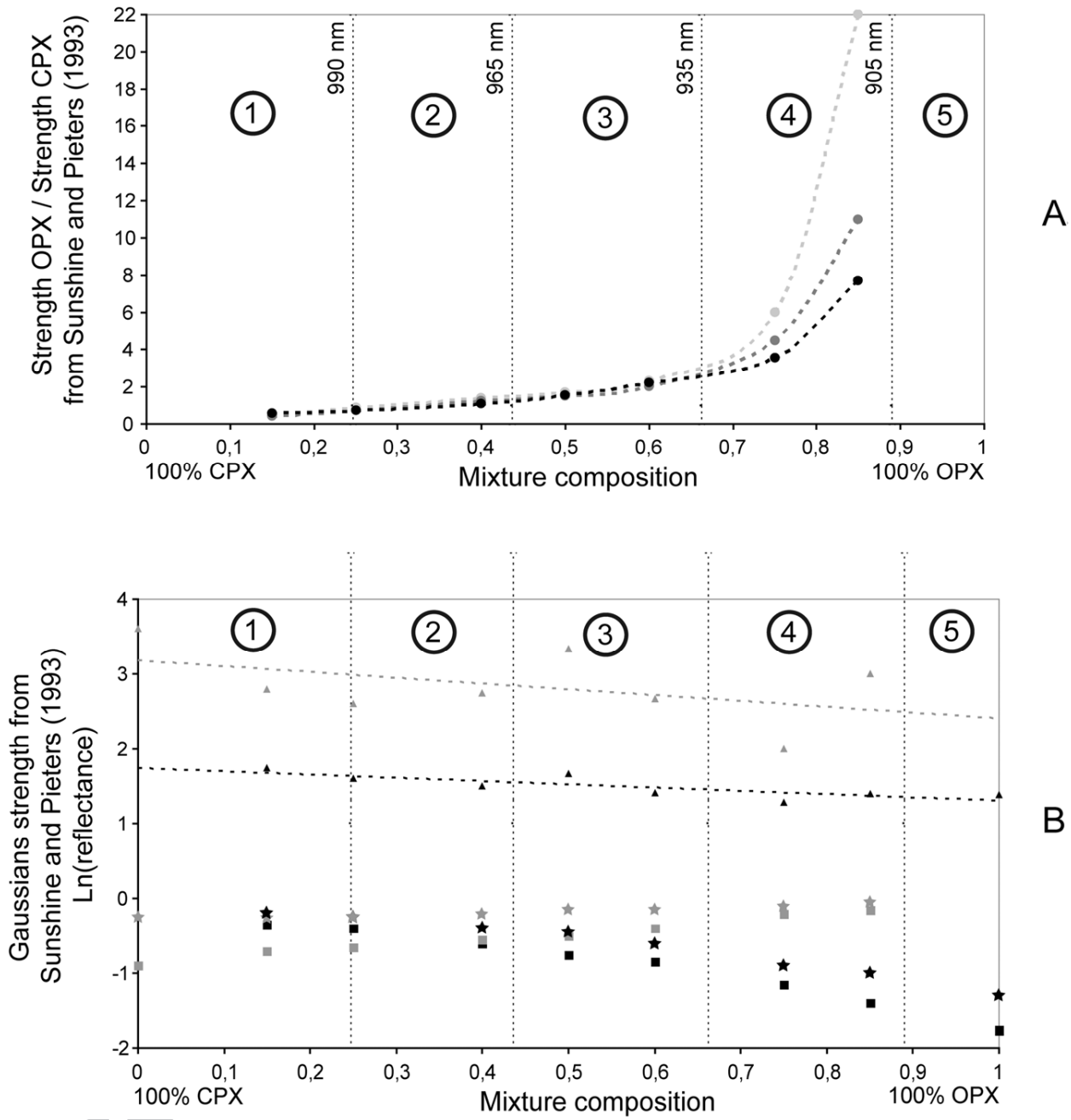
Strength OPX / Strength CPX from Sunshine and Pieters (1993)
990 nm
965 nm
935 nm
905 nm
1
2
3
4
5
100% CPX
Mixture composition
100% OPX
A
Gaussians strength from Sunshine and Pieters (1993) Ln(reflectance)
100% CPX
Mixture composition
100% OPX
B

Figure 4

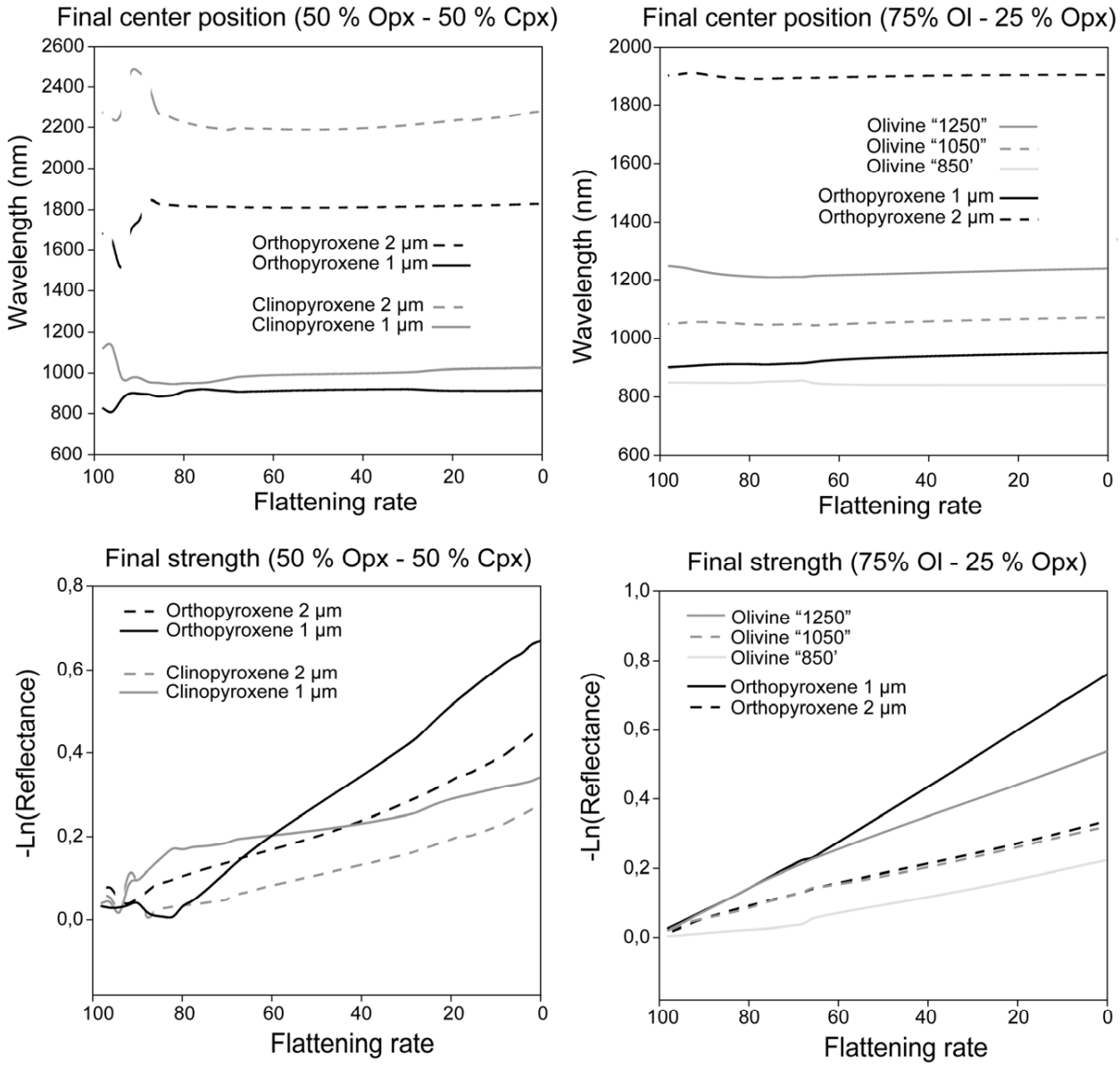

1142

1143 **Figure 5**

1144

1145

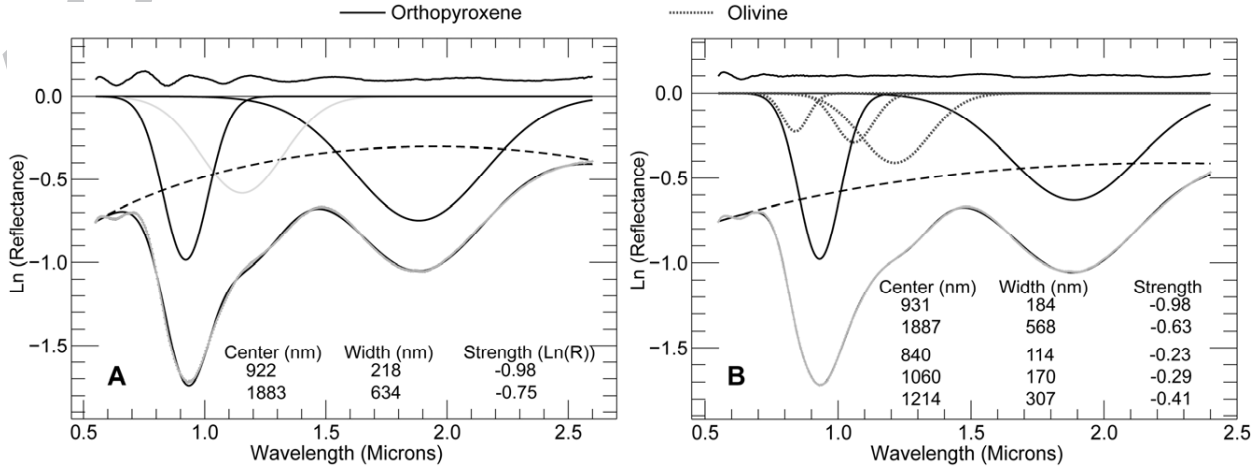

1146

1147 **Figure 6**

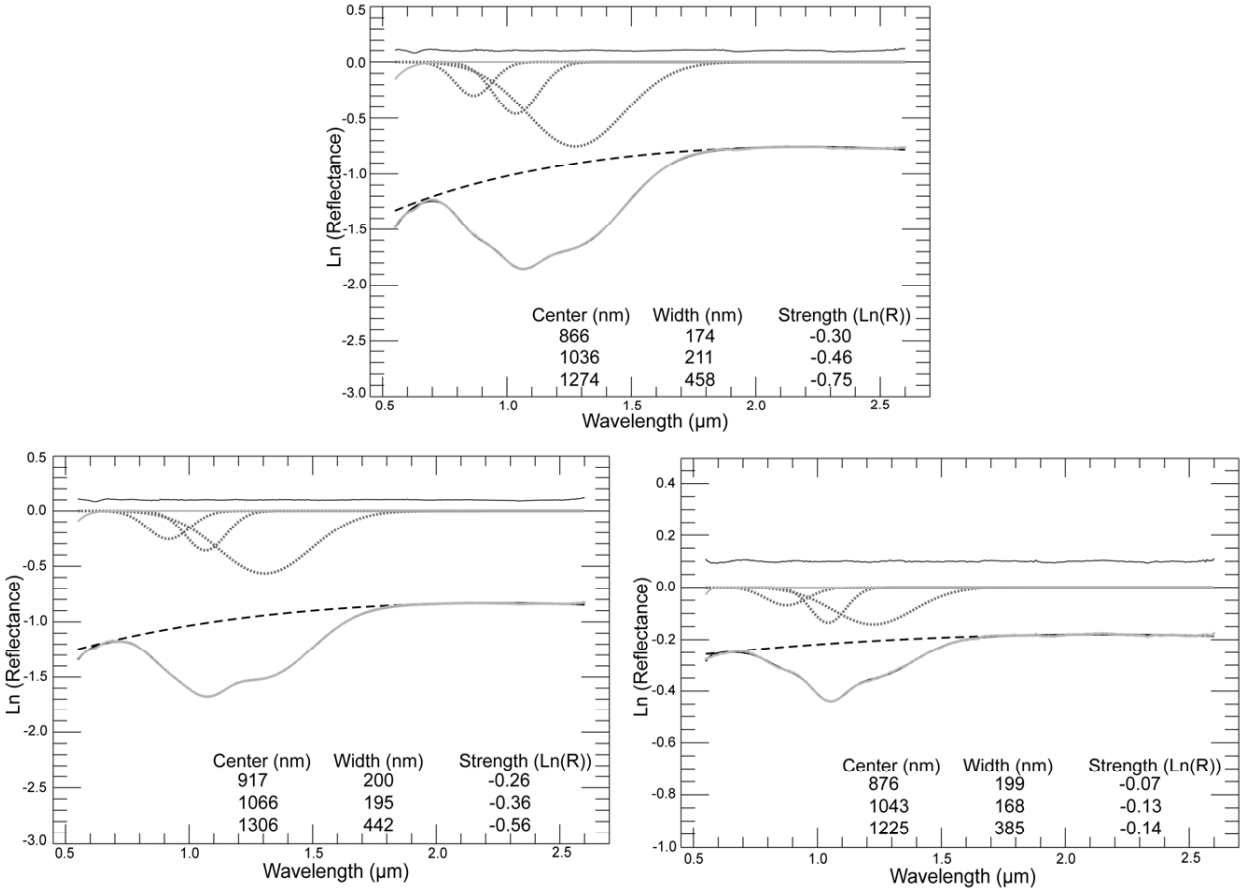

Figure 7

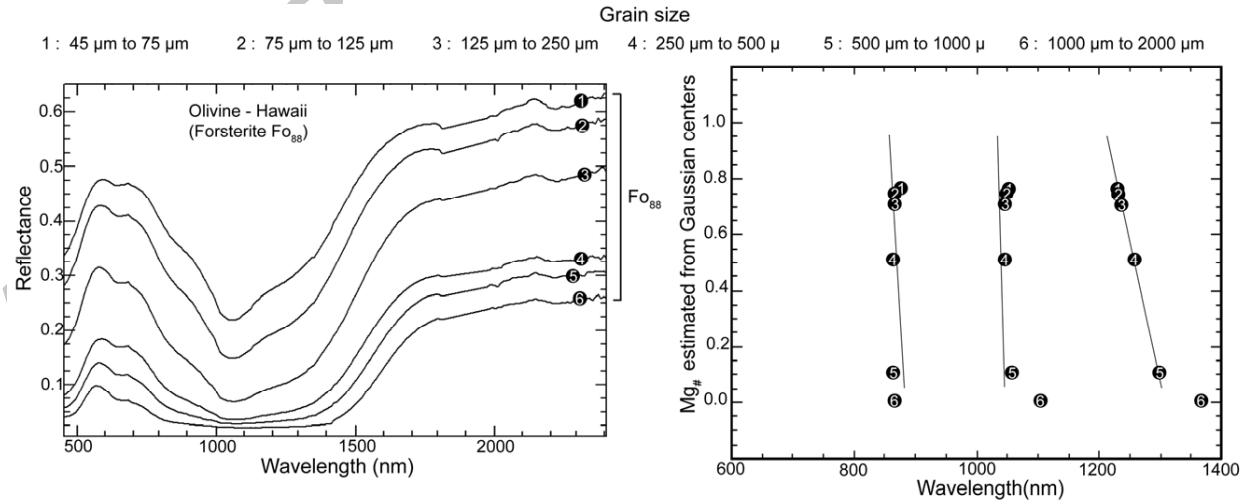

Figure 8

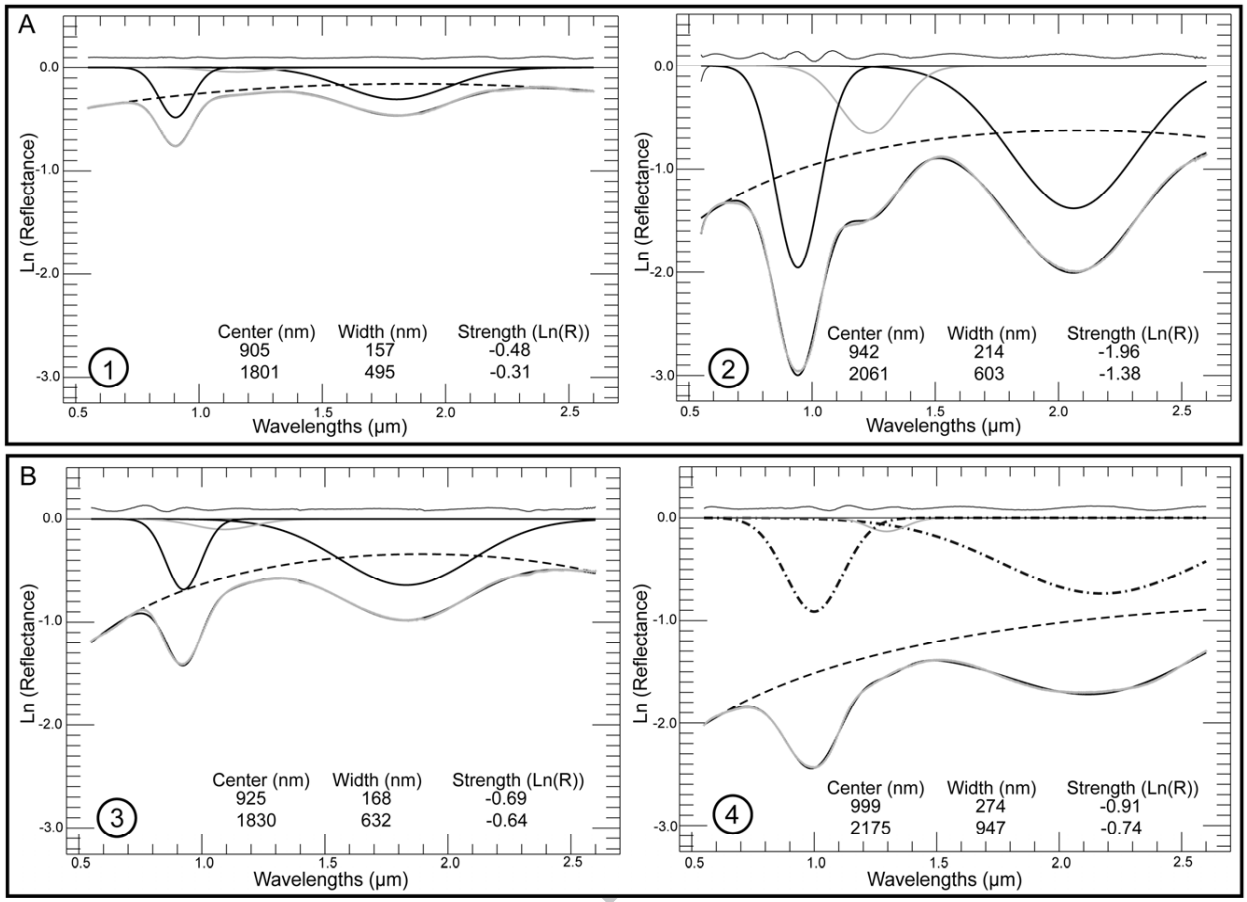

Figure 9

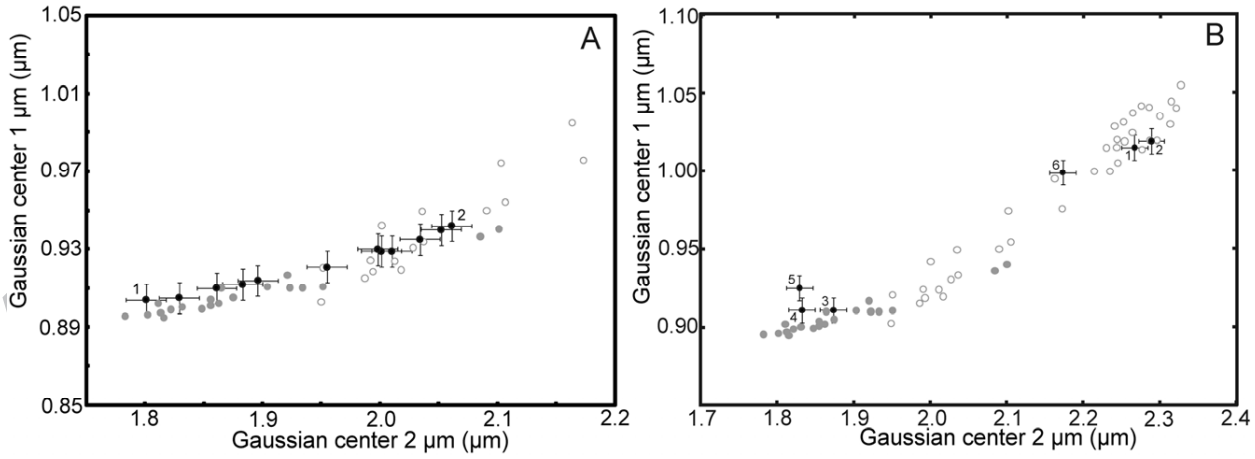

Figure 10

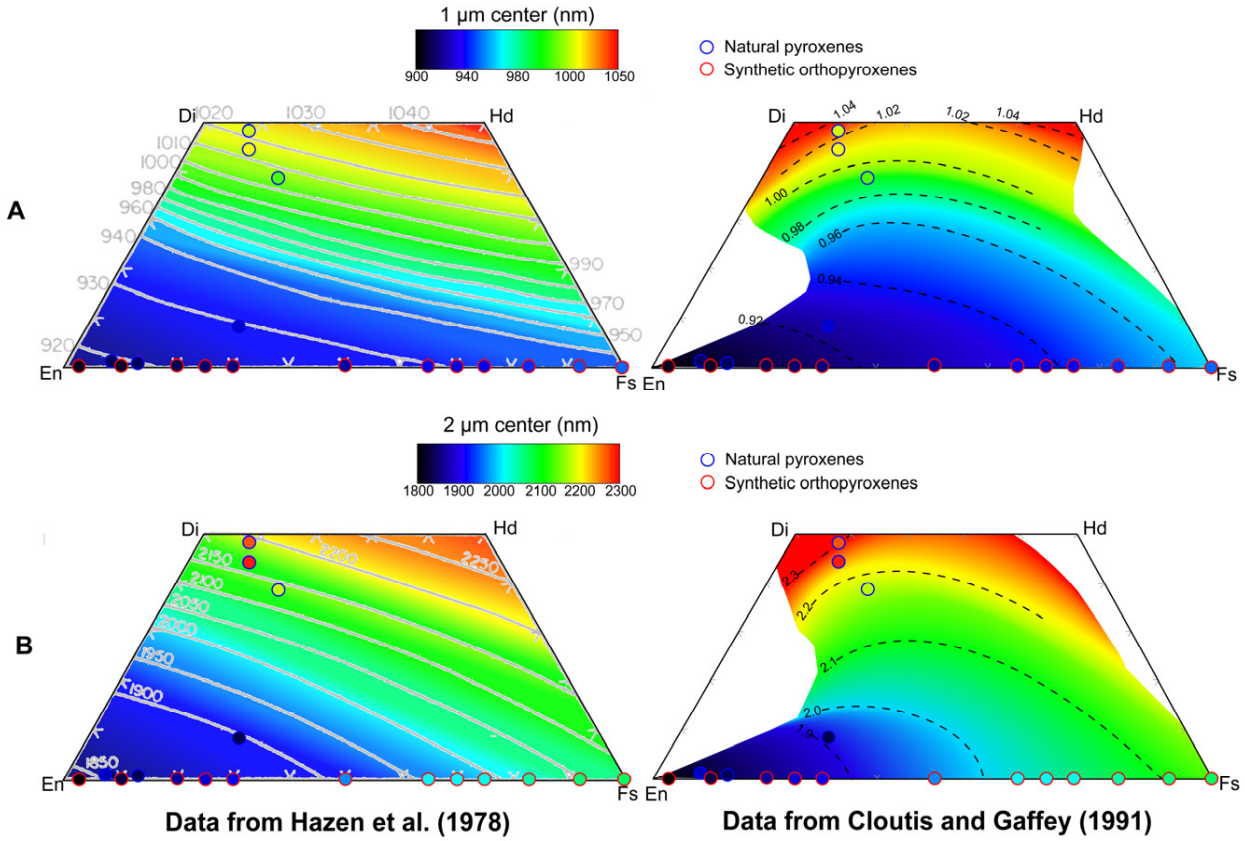

1162

1163 **Figure 11**

1164

1165

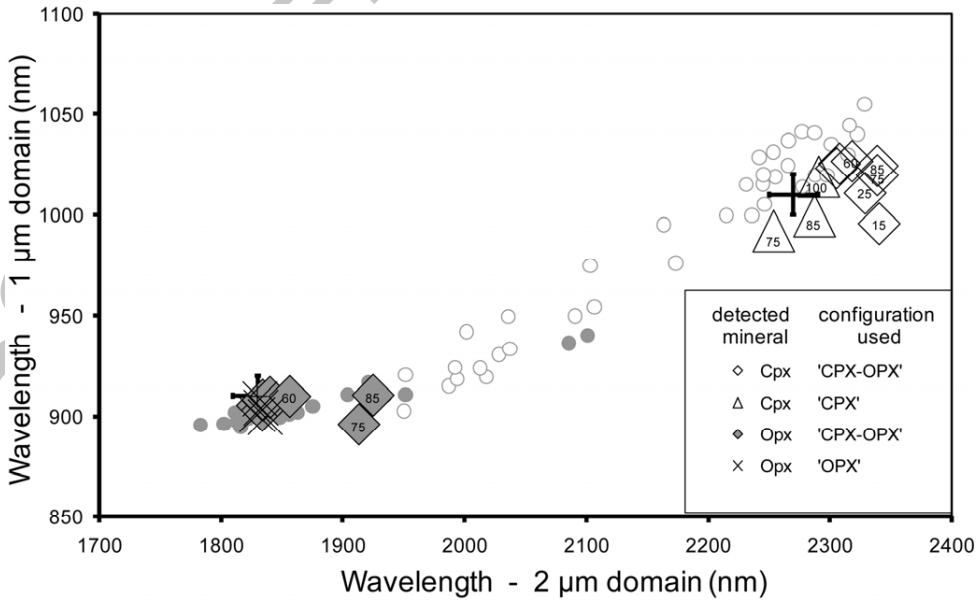

1166

1167 **Figure 12**

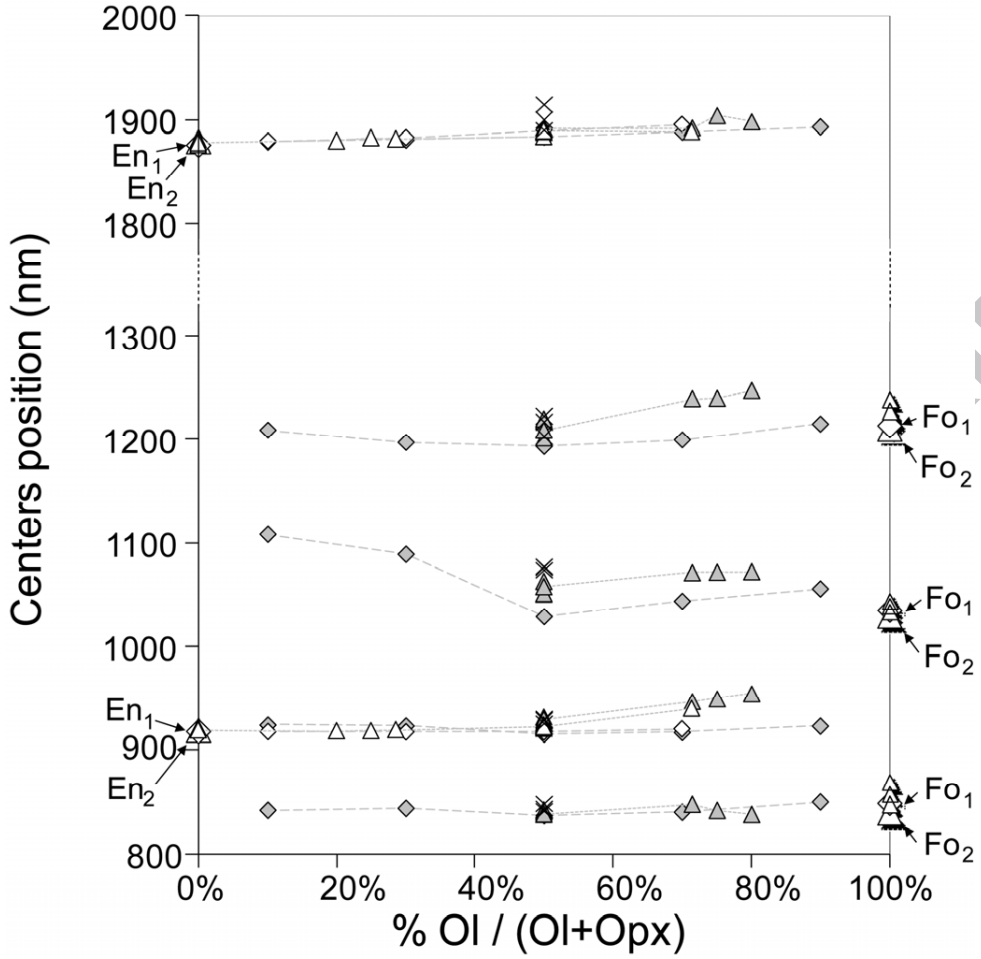

Figure 13

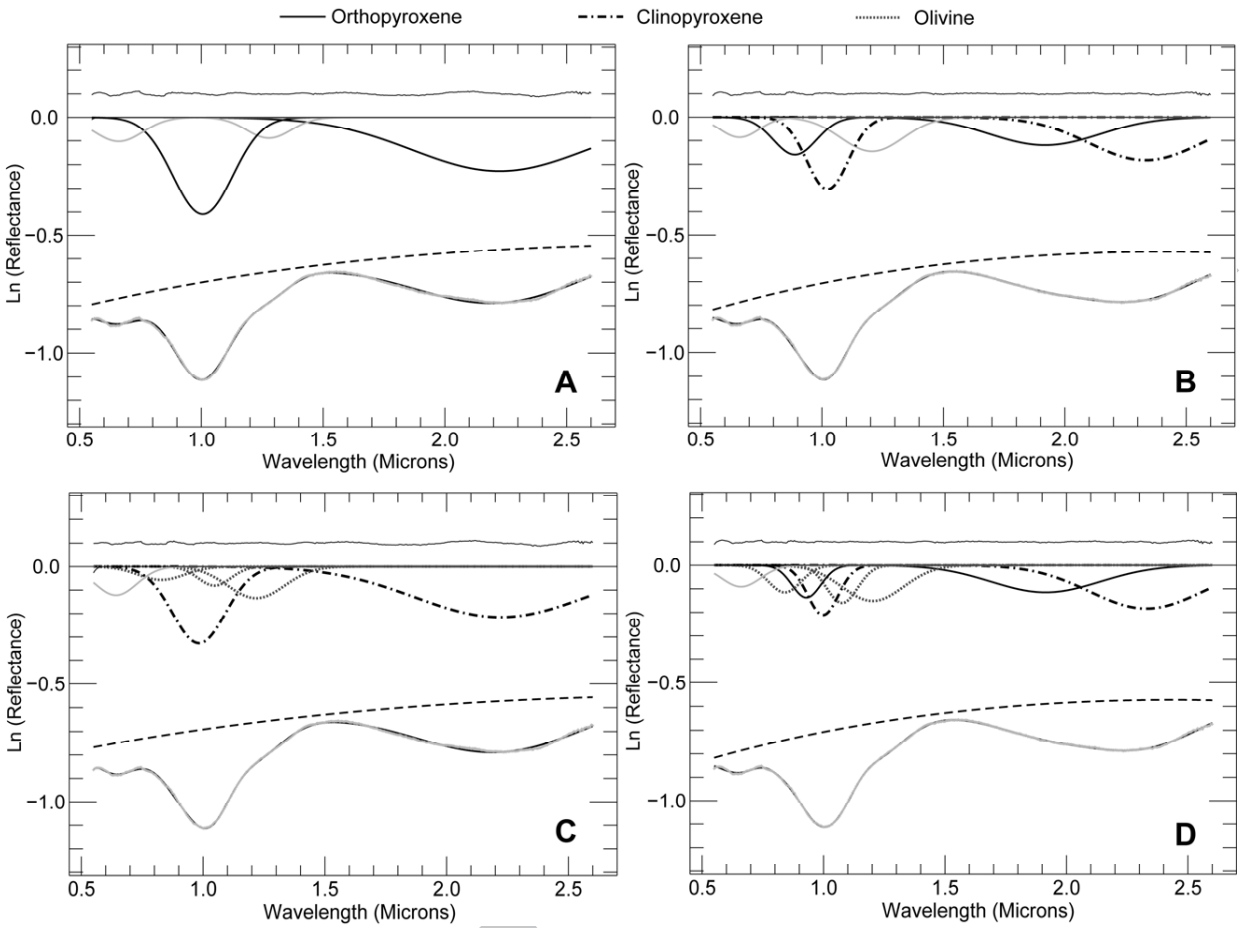

Figure 14

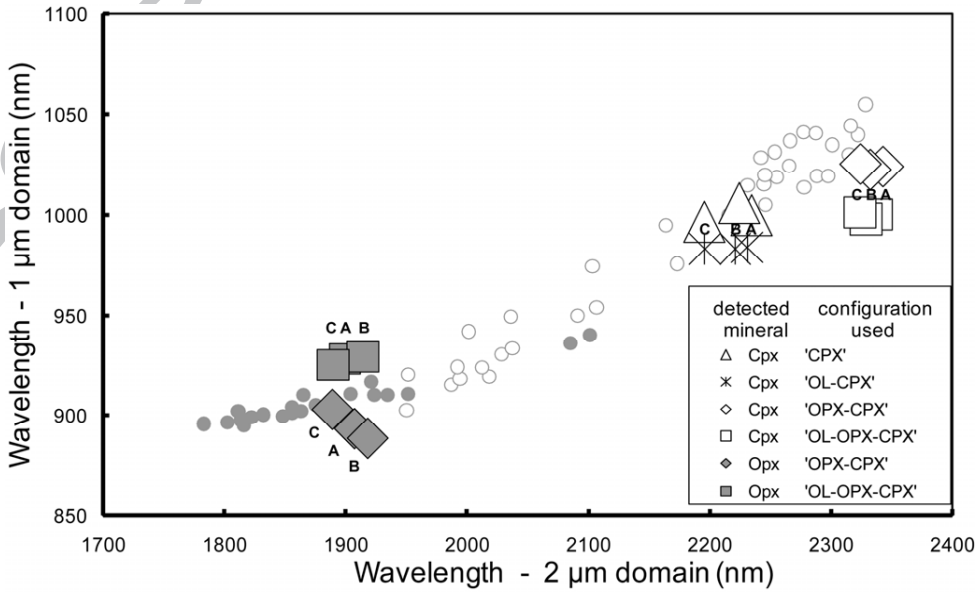

Figure 15

> Automatic procedure implemented on the original MGM approach
> Allow to deal with complex mineralogies involving olivine and/or pyroxene(s)
> Demonstration on binary and ternary mixtures with different chemical compositions
> Interpretation of MGM outputs in terms of modal and chemical compositions